

Glacial areas, lake areas, and snowlines from 1975 to 2012

M. N. Hanshaw and
B. Bookhagen

Glacial areas, lake areas, and snowlines from 1975 to 2012: status of the Cordillera Vilcanota, including the Quelccaya Ice Cap, northern central Andes, Peru

M. N. Hanshaw and B. Bookhagen

Department of Geography, University of California, Santa Barbara, USA

Received: 14 December 2012 – Accepted: 13 February 2013 – Published: 25 February 2013

Correspondence to: M. N. Hanshaw (mnhanshaw@geog.ucsb.edu)

Published by Copernicus Publications on behalf of the European Geosciences Union.

Title Page

Abstract

Introduction

Conclusions

References

Tables

Figures



Back

Close

Full Screen / Esc

Printer-friendly Version

Interactive Discussion

Abstract

Glaciers in the tropical Andes of southern Peru have received limited attention compared to glaciers in other regions (both near and far), yet remain of vital importance to agriculture, fresh water, and hydropower supplies of downstream communities. Little is known about recent glacial-area changes and how the glaciers in this region respond to climate changes, and, ultimately, how these changes will affect lake and water supplies. To remedy this, we have used 144 multi-spectral satellite images spanning almost four decades, from 1975–2012, to obtain glacial and lake-area outlines for the understudied Cordillera Vilcanota region, including the Quelccaya Ice Cap. In a second step, we have estimated the snowline altitude of the Quelccaya Ice Cap using spectral unmixing methods. We have made the following four key observations: first, since 1988 glacial areas throughout the Cordillera Vilcanota have been declining at a rate of $5.46 \pm 1.70 \text{ km}^2 \text{ yr}^{-1}$ (22-yr average, 1988–2010, with 95 % confidence interval). The Quelccaya Ice Cap, specifically, has been declining at a rate of $0.67 \pm 0.18 \text{ km}^2 \text{ yr}^{-1}$ since 1980 (31-yr average, 1980–2011, also with 95 % confidence interval); Second, decline rates for individual glacierized regions have been accelerating during the past decade (2000–2011) as compared to the preceding decade (1990–2000); Third, the snowline of the Quelccaya Ice Cap is retreating to higher elevations as glacial areas decrease, by a total of almost 300 m between its lowest recorded elevation in 1989 and its highest in 1998; and fourth, as glacial regions have decreased, 61 % of lakes connected to glacial watersheds have shown a roughly synchronous increase in lake area, while 84 % of lakes not connected to glacial watersheds have remained stable or have declined in area. Our new and detailed data on glacial and lake areas over 37 yr provide an important spatiotemporal assessment of climate variability in this area. These data can be integrated into further studies to analyze inter-annual glacial and lake-area changes and assess hydrologic dependence and consequences for downstream populations.

Glacial areas, lake areas, and snowlines from 1975 to 2012

M. N. Hanshaw and
B. Bookhagen

Title Page

Abstract

Introduction

Conclusions

References

Tables

Figures



Back

Close

Full Screen / Esc

Printer-friendly Version

Interactive Discussion



1 Introduction

Glaciers are thought of as excellent indicators of climate change, as small climate variations can produce rapid glacial changes (e.g., Soruco et al., 2009; IPCC, 2007; Vuille et al., 2008a; Rabatel et al., 2013). Changes to polar glaciers as a result of climate change have received widespread attention; however, changes to tropical glaciers, such as those found in the central Andes of South America have traditionally received less attention. Changes to small tropical glaciers are difficult to predict as the coarse resolution of global climate models makes resolving the steep topography of mountain areas difficult (Vuille et al., 2008a). Yet consequences of glacial retreat and mass-balance loss as a result of warming trends may be felt much sooner in the central Andes than in polar regions: the current state and future fate of Andean glaciers and seasonal snow cover are of central importance for the water, food, and power supplies of densely populated regions in countries including Peru and Bolivia (Kaser et al., 2010; Barnett et al., 2005; Bradley et al., 2006). Despite heavy dependence on the seasonal buffering provided by Andean glacial meltwaters (e.g., ~80% of Peru's energy is hydropower) (Vergara et al., 2007), observation and understanding of these terrestrial water stores and fluxes remains poor. Additionally, glacial retreat not only has consequences for water supplies, but also related natural hazards, including avalanches and glacial lake outburst floods (GLOFs), which are likely to become more common (Huggel et al., 2010, 2002; Carey, 2005).

As in polar regions, glaciers in many parts of the tropical Andes are retreating and losing mass (IPCC, 2007; Vuille et al., 2008a; Bradley et al., 2006; Rabatel et al., 2013). In this region, mass-balance studies are extremely rare and both spatially and temporally limited (Vuille et al., 2008b; Kaser and Georges, 1999; Thompson et al., 2006; Soruco et al., 2009; Rabatel et al., 2013). Consequently, little is known about the timescales and equilibrium conditions of the vast majority of tropical Andean glaciers, and how climate variability affects their mass balances. In Peru, most studies have focused on glaciers in the Cordillera Blanca, which represents the largest glacierized

TCD

7, 573–634, 2013

Glacial areas, lake areas, and snowlines from 1975 to 2012

M. N. Hanshaw and
B. Bookhagen

Title Page

Abstract

Introduction

Conclusions

References

Tables

Figures

⏪

⏩

◀

▶

Back

Close

Full Screen / Esc

Printer-friendly Version

Interactive Discussion

mountain range in the tropics (Georges, 2004; Silverio and Jaquet, 2005; Racoviteanu et al., 2008a). However, the second largest mountain range in Peru, the Cordillera Vilcanota (CV), south-east of the Cordillera Blanca (Fig. 1), has received much less attention to date. The CV is home to the Quelccaya Ice Cap (QIC), the Earth's largest tropical ice cap, one of the few sites of long-term glacier research in this region; Lonnie Thompson and his Ohio State University research group have been visiting and monitoring the ice cap since 1963. While Thompson and others (Thompson, 1980; Thompson et al., 1979, 1985, 2006; Brecher and Thompson, 1993; Hastenrath, 1998, 1978) have a long research history in the Quelccaya region, others are continuing research in this region also (e.g., Salzmann et al., 2013; Mark et al., 2002; Albert, 2002, 2007; Klein and Isacks, 1999).

As an icon of Andean glaciology and a region where glacial outlines are still minimal or lacking, for this study we have focused on the CV region and the QIC, where, according to Salzmann et al. (2013), “a comprehensive study on recent glacier changes is still lacking”. While their study begins to address this, our study goes further to fill the data paucity in this region by using a total of 144 multi-spectral satellite images to obtain glacier and lake area outlines in the CV region, in addition to approximating the snowline altitude of the QIC, for a time series that spans almost four decades (1975–2012). We detail the methods used to outline the glacierized areas in this region, in addition to many of the lakes, specifically proglacial, not subglacial or supraglacial lakes. In some previous lake classification studies, Huggel et al. (2002) investigated a method to delineate lakes for assessing the hazards of GLOFs in the Swiss Alps, while Wessels et al. (2002) focused on supraglacial lakes and the methods used to delineate those in the Himalaya. Gardelle et al. (2011) used a combination of the two methods to investigate proglacial and supraglacial lakes in the Himalaya, but as yet, no studies have focused on lakes in the CV of Peru. With populations highly dependent on the glaciers and their meltwaters, (in this case, specifically, the moderately densely populated region of Cusco; Salzmann et al., 2013), it is important to study how these lakes

Glacial areas, lake areas, and snowlines from 1975 to 2012

M. N. Hanshaw and
B. Bookhagen

[Title Page](#)[Abstract](#)[Introduction](#)[Conclusions](#)[References](#)[Tables](#)[Figures](#)[⏪](#)[⏩](#)[◀](#)[▶](#)[Back](#)[Close](#)[Full Screen / Esc](#)[Printer-friendly Version](#)[Interactive Discussion](#)

are changing with respect to the glaciers. The CV also extends into the Puno region of Peru, but predominantly provides water to the Cusco region.

We also investigated snowline changes for the QIC. Tropical glaciers behave differently than high-latitude glaciers, and the methods previously used to delineate the snowline or equilibrium line altitude (ELA) in other regions globally (Hall et al., 1987; Bronge and Bronge, 1999; Mathieu et al., 2009; Yu et al., 2012) proved unsuccessful in this region. It is difficult to delineate snow and ice on the glaciers and to outline the snowline, but this study follows on from methodology suggested for this region by Klein and Isacks (1999) using spectral unmixing to investigate snowline changes for the QIC.

Using the 144 multi-spectral satellite images, we (1) pre-processed the imagery (georeferenced and co-registered), (2) applied various classification methods to the imagery to best delineate glacial and lake area outlines, and (3) used spectral unmixing to distinguish between snow and ice on a glacier to approximate the change in the snowline of the QIC over time. Our results can ultimately be incorporated into the Global Land Ice Measurements from Space (GLIMS) database, and used by those seeking to develop methods to adapt to climate change in this region.

2 Geographic and climatic setting of the study site

The CV and the QIC are located in the central Andes in southeastern Peru (Fig. 1), specifically, in the southern portion of the eastern branch (Cordillera Oriental) of the Peruvian Andes (Hastenrath, 1998). We have used the general geographic definition of the CV as provided by Morales Arnao (1998), and in this study we refer to this as the entire CV study area. The CV mountain range is among the highest in Peru, with the highest peak (Nevado Ausangate) at 6384 m a.s.l. (above sea level), and glaciers terminating around 4700–5000 m a.s.l. (Salzmann et al., 2013). Climatically, the CV region experiences one thermal season with nearly constant temperatures and high solar radiation (Rabatel et al., 2012) throughout the year, but a distinctive precipitation season (October/November to March/April) followed by a dry season (April/May

Glacial areas, lake areas, and snowlines from 1975 to 2012

M. N. Hanshaw and
B. Bookhagen

Title Page

Abstract

Introduction

Conclusions

References

Tables

Figures

⏪

⏩

◀

▶

Back

Close

Full Screen / Esc

Printer-friendly Version

Interactive Discussion



to September/October) (Vuille et al., 2008b; Rabatel et al., 2013) with a similar seasonality of humidity (Rabatel et al., 2012). Most of the precipitation falls during the wet season, the glacier accumulation season. Ablation, however, while more dominant during the April to November dry season, also occurs year round due to the high solar radiation and constant temperatures at the high altitudes of the CV (Vuille et al., 2008a). Additionally, on interannual timescales, the El Niño Southern Oscillation (ENSO) is reported to have a significant influence on the climate in this region (Vuille et al., 2008a; Albert, 2007; Rabatel et al., 2013; Salzmann et al., 2013), with La Niña years tending to be cooler and wetter, and El Niño years tending to be warmer and dryer (Vuille et al., 2008a; Rabatel et al., 2013). How this affects glacier mass balance in the CV, however, has yet to be systematically investigated. The regions in southeastern Peru are characterized by a very steep precipitation gradient and orographic rainfall effect created by the eastern Andean slopes (Bookhagen and Strecker, 2008) (Fig. 1c), ranging from $> 3 \text{ m yr}^{-1}$ annual rainfall at the mountain front to $< 0.25 \text{ m yr}^{-1}$ rainfall on the high-elevation, arid Altiplano.

3 Data sources

To create our glacial and lake area inventory, we used a variety of optical and multi-spectral satellite imagery, including Landsat Multi-Spectral Scanner (MSS), Thematic Mapper (TM) and Enhanced Thematic Mapper Plus (ETM+), Advanced Spaceborne Thermal Emission and Reflection Radiometer (ASTER), and declassified Corona KH-9 imagery. The characteristics of each of these sensors can be found in Table 1, and an example of each of these images can be seen in Fig. 2.

We have obtained a total of 108 usable Landsat images (6 MSS from 1975–1985, 96 TM from 1985–2011, 6 ETM+ from 1999–2003), 35 ASTER images (from 2001–2012), and 1 KH-9 Corona image from 1980, for a total of 144 images dating from 1975 to 2012. All 144 images were used to create a lake area time series, although not every lake was outlined in each image due to clouds or the occasional difficulty in classifying

Glacial areas, lake areas, and snowlines from 1975 to 2012

M. N. Hanshaw and
B. Bookhagen

Title Page

Abstract

Introduction

Conclusions

References

Tables

Figures

⏪

⏩

◀

▶

Back

Close

Full Screen / Esc

Printer-friendly Version

Interactive Discussion



Glacial areas, lake areas, and snowlines from 1975 to 2012

M. N. Hanshaw and
B. Bookhagen

Title Page

Abstract

Introduction

Conclusions

References

Tables

Figures

⏪

⏩

◀

▶

Back

Close

Full Screen / Esc

Printer-friendly Version

Interactive Discussion

a specific lake. 77 images (63 Landsat, 1 Corona, and 13 ASTER) were used to create the glacial area time series, with images containing a range of 1 to all (10 identified) of the glacierized regions located within this Landsat TM/ETM+ scene (Fig. 2a), as similarly to the lakes, not all images could be used for all glacierized regions due to classification problems. Specifically for this area, obstruction by cloud cover limits the images that can be used to the dry season (Rabatel et al., 2012), during which convective storms are more rare. However, storms producing transient snow cover do still occur during the dry season, and this local/regional snow can prevent obtaining accurate glacierized region outlines. For this reason, we have only used images, or parts of images (as this snow is often localized), where no transient snow cover exists. For more information regarding the images used, please refer to Table SM A1 in the Supplement.

In addition to the multi-spectral satellite imagery, this study used the 2000 Shuttle Radar Topography Mission (SRTM) Digital Elevation Model (DEM) (version 4). Acquired within 11 days during February 2000, this mission provided near-global ($\sim 60^\circ$ N to 56° S latitude) digital elevation data at a horizontal resolution of ~ 90 m (Farr et al., 2007). Linear vertical absolute and relative height errors are less than 16 m and 10 m respectively, decreasing to 6.2 m and 5.5 m respectively for South America (Farr et al., 2007). For this study, these data were resampled to 15 m using bilinear interpolation. We also worked with the ASTER Global Digital Elevation Model (GDEM V1 and V2), a DEM created from ASTER imagery taken over the course of a decade. Since glacial elevations are likely to change over 10-yr time periods, inconsistencies over glaciers and shadowing effects from topography and clouds prevented us from using the ASTER GDEM.

4 Methodology

The creation of lake, glacier, and snowline outlines are multi-step processes with some manual intervention. Upon acquisition, and before classification, the images require initial pre-processing and calibration. This involves georeferencing (Corona, ASTER),

Glacial areas, lake areas, and snowlines from 1975 to 2012

M. N. Hanshaw and
B. Bookhagen

Title Page

Abstract

Introduction

Conclusions

References

Tables

Figures

⏪

⏩

◀

▶

Back

Close

Full Screen / Esc

Printer-friendly Version

Interactive Discussion

pan-sharpening (base-image only), resampling if necessary (ASTER Short Wave Infra-Red (SWIR) 30 m to 15 m), conversion to reflectance (all ASTER images, and Landsat images used for snowline analysis, converted to reflectance using standard techniques), and aligning to the base image (all images). For this study, a Landsat ETM+ image from 24 June 2000 (path 003, row 070, Fig. 2a) was chosen as the base image as this image covered the entire study region with no clouds and good gain control, important factors when aligning images or calibrating images for reflectance. We specifically used a Landsat ETM+ image for this, as Masek et al. (2001) report that Landsat ETM+ has decreased noise levels and increased radiometric precision compared to Landsat TM 5.

The general process used to classify the images is outlined in Fig. 3. Upon completion of pre-processing, the first step was to classify the lakes in each image, i.e. to create a lake mask (Sect. 4.1). This was done using simple band ratios and filtering, removal of shadows using a hillshade mask for each image, followed by manual editing (Huggel et al., 2002). Glaciers were classified similarly using simple ratios (Svoboda and Paul, 2009) (Sect. 4.2). Subsequently, the previously created lake mask was applied to the ratio image, to remove incorrectly classified lakes. Manual editing and validation was a required final step. In determining the snowline for a particular glacier (Sect. 4.3), a calibrated reflectance image was first clipped to the glacier extent using this glacier mask. After selecting snow and ice regions, we then performed a Multiple Endmember Spectral Mixture Analysis (MESMA) (Klein and Isacks, 1999; Roberts et al., 1998). To create files usable in further analysis, all rasters are converted to polygons.

4.1 Lake area mapping

Our primary purpose of lake extraction is to correct and refine glacial mapping by outlining proglacial lakes in the imagery. The steps involved in the lake classification of each group of imagery are summarized in Fig. 4 and outlined in detail in Appendix B1 of the Supplement.

Glacial areas, lake areas, and snowlines from 1975 to 2012

M. N. Hanshaw and
B. Bookhagen

Title Page

Abstract

Introduction

Conclusions

References

Tables

Figures

⏪

⏩

◀

▶

Back

Close

Full Screen / Esc

Printer-friendly Version

Interactive Discussion

Lakes in glacial regions often have a variety of biological and physical components (e.g., pollen and sediment) influencing their color, and the employed methodology must be able to distinguish varying colors. For the Landsat TM/ETM+ imagery we pursued the methodology outlined in Huggel et al. (2002) using the Normalized Difference Water Index (NDWI: Landsat bands (TM4-TM1)/(TM4+TM1)) followed by a hillshade mask. This NDWI performed well to classify lakes with a range of suspended sediment concentrations. ASTER images were processed in the same fashion as the Landsat TM/ETM+ images, however, they proved more complicated due to their lack of a “blue” band (0.45–0.52 μm , equating to Landsat B1, see Table 1). Previous studies have used the green band as an alternative, resulting in an approximation of the NDWI algorithm using (AST3-AST1)/(AST3+AST1) (Bolch et al., 2008). While this index performed fairly well to identify lakes with higher concentrations of suspended sediment (typically found in close proximity to glaciers), it was unable to capture lakes with lower concentrations of suspended sediment as successfully. To classify lower sediment content lakes, a threshold in ASTER B3 proved successful, but alternatively was not always successful at identifying the higher sediment content lakes. A combination of both the ASTER NDWI-approximation algorithm and ASTER B3 provided the most suitable method to identify lakes with the greatest range of suspended sediment concentrations. Unfortunately, this combination method could not identify all lakes throughout the study region. Figure 5 outlines the method used to classify lakes in the ASTER imagery, illustrating where each method works and does not work.

After initial classification and filtering, shadows were removed using a hillshade mask and some manual editing, resulting in a master lake file containing only lakes for each image. We then selected, and manually quality controlled, fifty lakes that were typically well classified (large and small, high and low sediment concentrations, near and far from glaciers, representing a range of lakes). The methods, thresholds and filters used in the classification of lakes and glaciers for each data set are summarized in Table 2.

4.2 Glacier area mapping

Debate continues on the best method to be used for delineating glacial outlines, with different studies suggesting different methods as superior (Paul and Kääb, 2005; Racoviteanu et al., 2009, 2008b). The consensus that seems to have been reached is that it depends on the test site in question. Manual delineation is very time consuming and can be highly subjective. Band ratios and thresholds provide the best compromise between processing time and accuracy, with an estimated accuracy difference of < 3% between the three most often used techniques: Landsat bands 3/5, 4/5, and the Normalized Difference Snow Index (Albert, 2002). In our study, we followed the methodology outlined in Svoboda and Paul (2009) using Landsat (TM/ETM+) bands 3/5 and ASTER bands 3/4, followed by a threshold in Landsat and ASTER bands 1 to include snow and ice in cast shadow. Their MSS classification scheme worked poorly for our images, and so we classified the glacierized areas in the MSS images using a single-band thresholding process. Unfortunately, this method provides only a minimum areal extent, as snow and ice in shadow are completely ignored. The glaciers in the Corona and ASTER images lacking SWIR bands were manually delineated. While not all images are suitable for glacier classification (local/regional snow cover or clouds obscuring outlines), our study classified as many images as possible to gain as much information as possible on how the glacierized regions behave on an annual as well as a decadal time scale. The general steps involved in the glacier classification of each group of imagery are summarized in Fig. 6, with the methods and thresholds used for each set of imagery summarized in Table 2.

Upon creation of the initial glacier mask, post-classification and filtering, the previously created lake masks for each image were applied to each glacier mask to remove incorrectly classified lake pixels. Subsequently, polygons with areas $\leq 10\,000\text{ m}^2$ (corresponding to 11, 44, 2, and 177 pixels for Landsat TM/ETM+, ASTER, Landsat MSS and Corona, respectively) were removed (as recommended by Paul et al., 2009), as were any remaining lake polygons. Using the earliest images (two MSS images from

Glacial areas, lake areas, and snowlines from 1975 to 2012

M. N. Hanshaw and
B. Bookhagen

Title Page

Abstract

Introduction

Conclusions

References

Tables

Figures

⏪

⏩

◀

▶

Back

Close

Full Screen / Esc

Printer-friendly Version

Interactive Discussion



Glacial areas, lake areas, and snowlines from 1975 to 2012

M. N. Hanshaw and
B. Bookhagen

Title Page

Abstract

Introduction

Conclusions

References

Tables

Figures

⏪

⏩

◀

▶

Back

Close

Full Screen / Esc

Printer-friendly Version

Interactive Discussion

1975) we identified and assigned a unique ID to discrete glacierized areas (closed ice masses or polygons that are nearby or that appeared to be part of that same glacierized mass) throughout the Landsat TM/ETM+ scene extent encompassing the entire CV area. Working in chronological order from 1975 to 2011, these IDs were assigned to polygons falling within those of their earliest outline (the assumed largest glacierized area). For each image, we have only included those glacierized areas if the entire outlines are completely unobstructed by clouds or obscured by local snow. Similar to Salzmann et al. (2013), we have not separately mapped debris covered glaciers as these areas are expected to be minimal in this region. A more detailed description of the glacier classification process can be found in the Supplement (Appendix B2).

4.3 Snowline mapping

On some images from the mid-late ablation season, the snowlines are clearly visible. Classifying these snowlines, however, proved difficult. Many of the suggested methods proved unsatisfactory for this region, for example, Landsat TM bands 4/5 (Hall et al., 1987), Landsat TM bands 3/4 and 3/5, and maximum likelihood classification of principal components (Bronge and Bronge, 1999), maximum likelihood classification of principal components on ASTER imagery (Mathieu et al., 2009), and a two-step unsupervised classification process based on Landsat ETM+ bands and algorithms and snow/ice texture (Yu et al., 2012). While Rabatel et al. (2005) manually delineated the ELA on three glaciers in the French Alps, we pursued the methodology suggested by Klein and Isacks (1999) for the Zongo glacier in Bolivia and the QIC: spectral mixture analysis (e.g., Painter et al. 1998). Spectral unmixing has also been successfully used by Chan et al. (2009) in delineating the snowline and the area accumulation ratio for the Morteratsch glacier in Switzerland. In our study, we focus on the QIC, initially creating a spectral library of snow and ice endmembers per usable image. A small selection of these spectra was used to spectrally unmix the ice cap and delineate the snowline using Multiple Endmember (snow, ice, and shadow) Spectral Mixture Analysis (MESMA). The resulting classification identifies pixels that contain varying percentages of snow

and ice, allowing for classification of regions that are dominantly snow (accumulation zone) or dominantly ice (ablation zone). Performing this methodology (Fig. 7) on multiple images produced a time series for the snowline of the QIC. As with the lake and glacier classifications, more information on the snowline classification can be found in Appendix B3 of the Supplement.

All usable images (conditions were satisfactory in 17 images) were converted to reflectance and calibrated to the reflectance of the base image. After selecting representative endmember regions in each image, we used techniques described in Roberts et al. (2007) to create spectral libraries for each, and subsequently to identify optimum spectra for these endmembers, specifically using the metrics CoB (Count Based Endmember Selection), EAR (Endmember Average RMSE), and MASA (Minimum Average Spectral Angle). This resulted in 37 ice spectra and 8 snow spectra for our Landsat imagery. These optimized spectra, with their strong spectral differences between snow and ice that make this method robust (Fig. 8), were then run on each snowline image using MESMA.

Post-MESMA processing includes applying a threshold to the snow endmember classification, where regions with snow (rather than ice) were determined to be in pixels > 50% snow (this threshold was determined by visual examination, and corroborates what is estimated in another study; Chan et al., 2009). After filtering, the outline was converted to points and SRTM DEM values at those points extracted, to determine the elevation of the snowline.

5 Results

We first present our glacial results by focusing on the two largest glacierized regions in our study area: the Quelccaya Ice Cap (Glacial ID: 1), and the largest continuous (main) glacierized region in the Cordillera Vilcanota (Glacial ID: 2), in addition to results for the Cordillera Vilcanota as a whole. Results for three lakes follow (Lake IDs: 2 – Laguna Sibilacocha, 8 – unnamed, and 33 – proglacial lake of Qori Kalis in the QIC), after

Glacial areas, lake areas, and snowlines from 1975 to 2012

M. N. Hanshaw and B. Bookhagen

Title Page

Abstract

Introduction

Conclusions

References

Tables

Figures



Back

Close

Full Screen / Esc

Printer-friendly Version

Interactive Discussion



which we present our time series of the QIC snowline. Additional glacial and lake area results can be found in the Supplement (Appendix C1 and C2, respectively).

5.1 Glacier area changes

5.1.1 Quelccaya Ice Cap (QIC)

5 Our results indicate that the QIC has decreased in area by 42 % over the time period 1975–2011 (Fig. 10). Because the Landsat MSS data have lower spatial resolution and were classified using single band density slicing, we exclude the MSS data from our regression analysis (all regressions are unweighted). Between 1980 and 2011, an area of 15.5 km² of the QIC was lost (an area that represents 25 % of the 1980 QIC extent).

10 Using only the minimum area measurements for each year, this represents an average decline rate of $0.67 \pm 0.18 \text{ km}^2 \text{ yr}^{-1}$ (all uncertainties are 95 % confidence intervals unless otherwise noted). However, this decline has not been constant; our time series shows that there have been some important interannual variations in glacierized area – significant increases in glacierized area were observed during the early 2000s and more recently in 2011. Decline rates for the QIC increase in the 1990s and 2000s to $1.05 \pm 0.70 \text{ km}^2 \text{ yr}^{-1}$ and $1.09 \pm 0.53 \text{ km}^2 \text{ yr}^{-1}$, respectively (Table 3).

15 Glacial-area uncertainties (error bars) are calculated using perimeter and grid-cell size of imagery, following:

$$\text{Error (95\% confidence interval)} = (P/(G \cdot 0.6872/2)) \cdot G^2 \quad (1)$$

20 where P = perimeter and G = grid-cell size (spatial resolution).

5.1.2 Cordillera Vilcanota (CV)

Results for the remainder of the Cordillera Vilcanota reflect that of the Quelccaya Ice Cap: glacierized areas have been significantly decreasing over the time period 1975–2011. Specifically, the largest continuous (or main) glacierized region of the CV

Glacial areas, lake areas, and snowlines from 1975 to 2012

M. N. Hanshaw and
B. Bookhagen

Title Page

Abstract

Introduction

Conclusions

References

Tables

Figures

⏪

⏩

◀

▶

Back

Close

Full Screen / Esc

Printer-friendly Version

Interactive Discussion



Glacial areas, lake areas, and snowlines from 1975 to 2012

M. N. Hanshaw and
B. Bookhagen

Title Page

Abstract

Introduction

Conclusions

References

Tables

Figures

⏪

⏩

◀

▶

Back

Close

Full Screen / Esc

Printer-friendly Version

Interactive Discussion

mountain range (Glacial ID: 2, Fig. 11) has seen a reduction in area of 109.7 km^2 between 1985 and 2011 (40 % of its 1985 area). Additionally, this glacierized region has an approximately five-times higher decline rate from 1985–2010 than that of the QIC, declining an average of $3.32 \pm 0.74 \text{ km}^2 \text{ yr}^{-1}$ (using minimum areas). As with the QIC, this decline has not been constant and glacierized area temporally increased during the late 1990s and early 2000s, before continuing its overall decline (Fig. 11). The 1990s and 2000s have high decline rates for the main glacierized region of the CV (MGRCV), with decline rates of $4.69 \pm 2.44 \text{ km}^2 \text{ yr}^{-1}$ (1990–2000) and $4.89 \pm 1.72 \text{ km}^2 \text{ yr}^{-1}$ (2000–2011). For this particular glacierized region, Landsat MSS images seemed to underestimate the extent of the glacierized area, likely due to increased shadow regions in the images used.

In the 22 yr between 1988 and 2010 (using only Landsat TM/ETM+ imagery), all glacierized regions throughout the entire Cordillera Vilcanota (Glacial IDs 1–7, 9–10, but not ID 8) declined by a total of 118.7 km^2 (32 % of 1988 extents). Including the MSS value from 1985 (likely an underestimate), this total decline increases to 35 % between 1985 and 2010 (Fig. 12). In Fig. 12 we also include data reported for the CV by Salzmänn et al. (2013) to (1) illustrate how our measurements align with respect to their measurements (our measurements correspond well, within the error bars, of their 1996 and 2006 measurements, however, our 1985 measurement is somewhat below theirs, although we note that ours is likely an underestimate), and (2) to illustrate how the use of multiple images and measurements, as used in this study, provides much more information on glacial decline and advance over this time period. For example, note the steep decrease in glacial area throughout the entire CV during 1998, which would be uncaptured were fewer measurements obtained. The table insets in Fig. 12 compare our decline rates to those of Salzmänn et al. (2013), using our minimum values during the relevant time periods, rather than just 2 data points for each. For the 1962 value, we also use the measurement from Ames et al. (1989).

To summarize, for the time period of 1988 through 2010 (TM/ETM+ only), the decline rate throughout the CV was $5.46 \pm 1.70 \text{ km}^2 \text{ yr}^{-1}$ ($n=15$, $r^2 = 0.8$), ($5.50 \pm 1.89 \text{ km}^2 \text{ yr}^{-1}$

using MSS from 1985). This decline rate increased during the 1990s (1990–2000) to a decline rate of $12.51 \pm 11.83 \text{ km}^2 \text{ yr}^{-1}$ ($n = 6$, $r^2 = 0.6$), and then decreased slightly during the first decade of the 21st century (2000–2011), to a decline rate of $9.04 \pm 2.51 \text{ km}^2 \text{ yr}^{-1}$ ($n = 8$, $r^2 = 0.9$). However, these decline rates are for the entire CV area, which are dominated by the largest glacierized region (Glacial ID: 2). Each of the glacierized regions within the CV (IDs 1–7, 9–10), have declined at different rates (Table 3). For the individual glacierized regions we report mostly increasing decline rates during the 2000s (2000–2011) over those of the 1990s (1990–2000) (Fig. 13). We also note that on average, smaller glaciers have higher decline rates than larger glaciers (Fig. 13, Table 4).

5.2 Lake area changes

Our lake area time series (1975–2012) includes 50 lakes (Fig. 9). Here, we present the results of three characteristic proglacial lakes: an existing large proglacial lake (Laguna Sibilinacocha (Lake ID: 2), Fig. 14), and two recently formed (1985) proglacial lakes (Lake ID: 8, Fig. 15, downstream of Nevado Ausangate (Glacial ID: 3), and Lake ID: 33, Fig. 16, a proglacial lake in front of Qori Kalis glacier, QIC (Glacial ID: 1)). Additionally, Fig. 17 summarizes how eight lakes surrounding the QIC have been changing with respect to the QIC's glacial area. We present additional results for lake area changes in the Supplement (Appendix C2).

Unlike glacierized regions, proglacial lake areas vary more widely both temporally and spatially, reflecting a variety of different melting processes, including GLOFs. Laguna Sibilinacocha (Lake ID: 2, Fig. 9, Fig. 14) is a large (15-km long) lake extending south from the tongue of one of the southern glaciers in the MGRCV (Glacial ID: 2). This particular lake is used for hydropower generation (Salzmann et al., 2013). Already the second largest lake in this region (the first being Laguna Langui, at $\sim 54.5 \text{ km}^2$), Laguna Sibilinacocha increased in area by 12 % (from 25.3 km^2 to 28.2 km^2) between 1982 and 2011. The majority of this increase occurred during the mid-late 1990s, before

Glacial areas, lake areas, and snowlines from 1975 to 2012

M. N. Hanshaw and
B. Bookhagen

Title Page

Abstract

Introduction

Conclusions

References

Tables

Figures

⏪

⏩

◀

▶

Back

Close

Full Screen / Esc

Printer-friendly Version

Interactive Discussion

which the lake area was relatively stable, but after which the lake area has fluctuated more widely.

In contrast to Laguna Sibinacocha (Lake ID: 2), the proglacial Lake ID 8 beneath the Nevado Ausangate region did not exist before 1985 (Figs. 9 and 15). Since then, however, this lake has rapidly developed, beginning during the late 1990s but particularly during the early 2000s, growing at an average rate of $12,605 \pm 1030 \text{ m}^2 \text{ yr}^{-1}$. Since the beginning of 2010, however, it appears as though the lake area has begun to decline.

Similar results can be seen for Lake ID 33 (a proglacial lake in front of Qori Kalis glacier in the QIC) (Fig. 16). Growth of this lake has been previously documented (Brecher and Thompson, 1993; Thompson et al., 2006) and reflects the retreat of Qori Kalis glacier (Fig. 21). Both Thompson et al.'s (2006) 1991–2005 retreat rate of $\sim 60 \text{ m yr}^{-1}$ and this study's retreat rate of $\sim 67 \text{ m yr}^{-1}$ correspond with the time period during which this lake experienced the majority of its growth. The period 2000–2005 showed even greater lake growth than during the previous 9 yr since 1991. This reflects our findings in this study of the higher glacial decline rates during the 2000s than during the 1990s, and the related growth of this proglacial lake in correspondence to this. In general, we note that areas of proglacial lakes have typically been fairly constant for $\sim 15\text{--}20 \text{ yr}$ preceeding 2002. Since 2002, however, proglacial lake areas began to rapidly increase. For the 8 lakes surrounding the QIC (Fig. 17) we note that post-2002, after rapid lake area increases and decreases over short time intervals, the lake areas have been highly fluctuating, despite fairly constant decline in the QIC glacial area.

5.3 Snowlines

Remote sensing studies in recent years have used the transient snowline at the end of the ablation period, or end of summer snowline (EOSS), as a proxy for the equilibrium line altitude (ELA) of a given year (Klein and Isacks, 1999; Østrem, 1975; Mathieu et al., 2009; Clare et al., 2002). While previously the use of the snowline to estimate the ELA in the outer tropics was based on assumption of correlation, a recent study (Rabatel et al., 2012) confirms, with some caveats (specifically, the necessity of validation),

Glacial areas, lake areas, and snowlines from 1975 to 2012

M. N. Hanshaw and
B. Bookhagen

Title Page

Abstract

Introduction

Conclusions

References

Tables

Figures



Back

Close

Full Screen / Esc

Printer-friendly Version

Interactive Discussion



Glacial areas, lake areas, and snowlines from 1975 to 2012

M. N. Hanshaw and
B. Bookhagen

[Title Page](#)[Abstract](#)[Introduction](#)[Conclusions](#)[References](#)[Tables](#)[Figures](#)[⏪](#)[⏩](#)[◀](#)[▶](#)[Back](#)[Close](#)[Full Screen / Esc](#)[Printer-friendly Version](#)[Interactive Discussion](#)

that the highest altitude reached by the snowline over the course of the entire ablation season (not just the EOSS) may provide an estimate of the ELA for that year (although it is likely an underestimation). In this study, we used spectral unmixing methods to delineate transient snowline elevations for the QIC from 1988 to 2010 using Landsat TM and ETM+ imagery (Fig. 18). Conditions were suitable for this purpose in only 17 images. We observed large inter-annual fluctuations, with high median snowline elevations in the late 1990s. Figure 18 reports our results alongside those from previous studies, but only minimal snowline measurements exist in the literature, whether determined in situ or using remote sensing methods. For the QIC, the lowest altitude that the snowline reached using results from this study was in 1989 (22 September), with a median altitude of 5287 m a.s.l. In 1998 (15 September) it reached its maximum of 5582 m a.s.l., almost 300 m higher. In 2010 (16 September), our most recent measurement, the snowline had descended to 5432 m a.s.l., ~ 150 m above its minimum altitude in 1989. Unfortunately, because no field measurements of the ELA for the QIC exist during our period of study, we are unable to validate our results. However, based on the relationship between snowline altitude (SLA) and ELA as reported in Rabatel et al. (2012), our measurements are likely to represent minimum estimates of the ELA for the given years (as the SLA on satellite images tends to be an underestimate of the ELA; Rabatel et al., 2012). In Fig. 18 we have chosen only to indicate positive errors in response to the fact that these SLAs are minimum ELA estimates. The trend still indicates that the elevation of the transient snowline of the QIC is increasing, at an average rate of $2.8 \pm 4.5 \text{ m yr}^{-1}$ between 1988 and 2010 (Fig. 18). Our errors appear to be large, but they reflect the SLA surrounding the entire QIC and are surprisingly robust.

6 Discussion

We first discuss our glacial-area changes, followed by lake-area and snowline changes. We then provide a summary of our data and results. We emphasize problems and

used, and the long extent of the time series in this study and therefore suggest that our data are robust.

Additional discrepancies between glacial-area measurements are caused by the time of year the satellite image was taken. The more images in a given year, the more visible this trend is. The data density of several reliable satellite images per year for some years allows us to see the (inter-) annual fluctuations in glacierized area (Figs. 10, 11, and 20). We note increasing areas over the wet winter accumulation period and then declining areas throughout the course of the dry summer ablation period (Fig. 20 zooms into the 2005–2012 time period of Fig. 10). For example, in 2009, the area of the *entire* QIC (Figs. 10 and 20) varied by 5 km² (10%), from 48.7 km² on 8 May, the earliest usable image after the accumulation period, to 43.7 km² on 31 October, at the end of the ablation period. Six images over the course of 2009 document this steady decline. Although only 3 images exist for 2011, that year underwent an even more drastic decline of 11.1 km² (19%), from an area of 58.7 km² on May 14 to 47.6 km² on 3 September. This illustrates how area measurements can vary even up to 19% in a given year, and emphasizes how important it is to give the date of measurement when reporting area results for glacierized regions.

Our satellite-based measurements correspond fairly well with those from other studies (Table 5), with the exception of 1975. Visual examination indicates that the MSS density slice classification delineates the QIC well for this image. We do not know the date of the image used for Salzmann et al.'s (2013) study, and can only suggest that the date of the imagery used, and the extent of the area termed the QIC are different between our two studies. Kaser and Georges (1997) report that there was a period of glacial advance in the mid-1970s, and perhaps our 1975 area measurement reflects this.

Just as the QIC remains a classic and fairly well documented example of glacial retreat in this region, the Qori Kalis glacier in the QIC (cf. location in Fig. 19) has been extensively field studied by Thompson and others over the past 3 decades (Brecher and Thompson, 1993; Thompson et al., 2006). We compare (Fig. 21) our satellite-derived

Glacial areas, lake areas, and snowlines from 1975 to 2012

M. N. Hanshaw and
B. Bookhagen

[Title Page](#)[Abstract](#)[Introduction](#)[Conclusions](#)[References](#)[Tables](#)[Figures](#)[⏪](#)[⏩](#)[◀](#)[▶](#)[Back](#)[Close](#)[Full Screen / Esc](#)[Printer-friendly Version](#)[Interactive Discussion](#)

Glacial areas, lake areas, and snowlines from 1975 to 2012

M. N. Hanshaw and
B. Bookhagen

Title Page

Abstract

Introduction

Conclusions

References

Tables

Figures

⏪

⏩

◀

▶

Back

Close

Full Screen / Esc

Printer-friendly Version

Interactive Discussion

glacial extents to field measurements for the Qori Kalis glacier (Thompson et al., 2006). While there are some discrepancies that are likely a result of measurements taken at different times of the year, the overall patterns match. Although our study does not have measurements for Qori Kalis dating back to 1963, the trends in the data are similar.

Thompson et al. (2006) report a frontal retreat rate of $\sim 6 \text{ m yr}^{-1}$ for Qori Kalis during the 15 yr period from 1963–1978, and a ~ 10 fold increase during the next 14 yr, from 1991–2005 (a retreat rate of $\sim 60 \text{ m yr}^{-1}$). Our satellite-based study supports these findings, with a retreat rate of $\sim 9\text{--}10 \text{ m yr}^{-1}$ during the shorter time period 1980–1991, but a similar retreat rate of $\sim 67 \text{ m yr}^{-1}$ during the subsequent 14 yr period from 1991–2005. This retreat corresponds to the development of the proglacial lake (Lake ID: 33) shown in Fig. 16.

6.1.2 Cordillera Vilcanota (CV)

As with the QIC, different studies use differing extents of the CV region. As previously mentioned in Sect. 2, our study uses the geographic definition as provided by Morales Arnao (1998) and incorporates this study's Glacial IDs 1–7 and 9–10. Glacial ID 8 is located beyond the CV and is not included in measurements where we discuss the *entire* CV. For their definition of the CV extent, between 1985 and 2006, Salzmann et al. (2013) report a 33 % loss in glacierized area. Over a similar time frame, from 1988 to 2010, our study reports a 32 % loss in area. Our definition of the extent of the CV region may incorporate slightly differing glacierized regions, however, the trends are comparable.

For their definition of the CV, Salzmann et al. (2013) report high decline rates ($9.1 \text{ km}^2 \text{ yr}^{-1}$) from 1985–1996, with slower decline rates ($4.7 \text{ km}^2 \text{ yr}^{-1}$) from 1996–2006 and actually a slight growth rate ($0.2 \text{ km}^2 \text{ yr}^{-1}$) for the earlier period from 1962–1985, based on two images per time period (Fig. 12). Based on two images per time period, our data report a $3.4 \text{ km}^2 \text{ yr}^{-1}$ decline rate for the period 1985–1996 (a CV area of 390 km^2 on 26 August 1985 (Landsat MSS) and 353 km^2 on 21 June 1996 (Landsat TM)), and a higher decline rate of $6.0 \text{ km}^2 \text{ yr}^{-1}$ during the period 1996–2006 (a CV area of 293 km^2

Glacial areas, lake areas, and snowlines from 1975 to 2012

M. N. Hanshaw and
B. Bookhagen

Title Page

Abstract

Introduction

Conclusions

References

Tables

Figures

⏪

⏩

◀

▶

Back

Close

Full Screen / Esc

Printer-friendly Version

Interactive Discussion



on 19 July 2006 (Landsat TM)), although this rate is slightly lower ($5.3 \text{ km}^2 \text{ yr}^{-1}$) if a date a month earlier is used (300 km^2 on 17 June 2006). However, our data allows us to calculate decline rates from 1996–2006 using 7 images (using minimum areas for each year) for each glacial ID, which results in an average decline rate of $6.09 \pm 9.61 \text{ km}^2 \text{ yr}^{-1}$ ($r^2 = 0.2$). Again, we emphasize the necessity to include date measurements when reporting area measurements, as Fig. 20 shows that area measurements can even vary by up to 19% within a year.

Because results based on single images alone can be biased, we have chosen to calculate our decline rates using as many images in the specific time periods as possible. To obtain as accurate an estimate of the decline as possible, we have limited the images used to calculate these decline rates to those that represent the minimum area measured for that year. Unfortunately, multiple images do not exist for all glacial IDs for all years, and in these cases the minimum area measurement is actually the only measurement. As a result, decline rates are also minimum estimates. Additionally, we also omit the Landsat MSS images because of their coarser spatial resolution and fewer channels, and have therefore calculated decline rates only with the Landsat TM/ETM+ imagery, since consistency is maintained in methodology throughout this dataset from 1985 to 2011. We have calculated decline rates for three different time periods (Fig. 13, and Table 3 (not normalized against area) and Table 4 (normalized against median area of each glacial ID's earliest Landsat TM outline). Our study finds that area-normalized decline rates for the majority of glacierized regions investigated (8 of 10) are highest during the period 2000–2011. The 1990s still showed high decline rates with 7 out of 10 glacierized regions reporting higher decline rates during the 1990s than over the course of the entire time period (Fig. 13 and Table 3). However, our results do support other studies which report higher decline rates during the 1990s when we calculate decline rates for the entire CV as a whole (a 1990–2000 decline rate of $12.51 \pm 11.83 \text{ km}^2 \text{ yr}^{-1}$ ($r^2 = 0.6$), and a 2000–2011 decline rate of $9.04 \pm 2.51 \text{ km}^2 \text{ yr}^{-1}$ ($r^2 = 0.9$)). These decline rate patterns are different to those for individual glacierized areas alone because the largest areas dominate the decline rates when calculated as a whole. With respect

Glacial areas, lake areas, and snowlines from 1975 to 2012

M. N. Hanshaw and
B. Bookhagen

Title Page

Abstract

Introduction

Conclusions

References

Tables

Figures

⏪

⏩

◀

▶

Back

Close

Full Screen / Esc

Printer-friendly Version

Interactive Discussion

to size, the majority of the smallest glacierized regions ($< \sim 12\text{--}20 \text{ km}^2$) show the overall highest area-normalized decline rates, particularly from 2000–2011 (Fig. 13 and Table 4). Our study presents decline rates deduced from a minimum of 16, and a maximum of 24, images over the time period 198X to 2011 for each glacierized region, which show a strong increase in areal decline rates. (If we were to use all images rather than only the minimum area images for each year, the number of images would increase to 31 and 63, respectively.) This increase in areal decline rates is an important finding, as other studies suggest that decline rates have been decreasing since the mid-1980s to mid-1990s, although they are likely using the region as a whole to calculate their decline rates. Our study suggests that decline rates are not decreasing, but instead are increasing for most glacierized areas in the CV region compared to the 1980s and 1990s.

We investigated the areal glacial retreat behavior with respect to elevation by analyzing the median elevation of a glacier through time. We observed that all median glacial elevations rose through time, but their rates differed with respect to elevation (Fig. 22). Glacierized areas with lower median elevations are retreating faster than glacierized areas at higher elevations (Fig. 22). For the 4 largest glacierized areas ($> 20 \text{ km}^2$) in the CV and just beyond, the median elevation gain ranged from $1.77 \pm 0.43 \text{ m yr}^{-1}$ to $2.91 \pm 0.51 \text{ m yr}^{-1}$. Median glacial elevations around 5200 m a.s.l. have been retreating to higher elevations at a rate of about 1 m yr^{-1} faster than glaciers located only 200 m higher at 5400 m a.s.l. These results reflect those found in Rabatel et al. (2013), specifically, that glaciers lower than 5400 m a.s.l. have been losing mass at a greater rate ($1.2 \text{ m w.e. yr}^{-1}$ (meters of water equivalent yr^{-1})) than those glaciers located higher than 5400 m a.s.l. ($0.6 \text{ m w.e. yr}^{-1}$). The majority of glaciers in this region terminate around 4700–5000 m a.s.l. (Salzmann et al., 2013) and will thus retreat more rapidly to higher elevations before retreat rates are likely to decrease.

6.2 Lake area changes

No studies exist examining proglacial and glacier-fed lake area changes in the northern central Andes. This is the first regional study summarizing lake area changes derived from satellite imagery. The majority of lakes in this region that we tracked have been small: 41 out of 50 (or 82 %) are less than 2 km², and only 3/50 (or 6 %) are larger than 5 km². Smaller lakes have larger errors associated with their area measurements, and many of our identified lakes fluctuate widely. This is likely a result of unstable lake areas, classification methodology, and the fact that many images required different thresholds to visually outline the same lake area. These factors make interpreting a signal through time difficult. However, some lakes show clear signals, particularly the proglacial lakes, of which we have shown the results specifically for three in this study (Figs. 14, 15, and 16) in addition to those surrounding the QIC (Fig. 17). In this study we focus on the lakes that are not readily affected by size limitations and classification thresholds.

We observed the rapid development of two proglacial lakes since 1985 that previously did not exist (Figs. 15 and 16). The development of these lakes reflects glacial retreat in this region, with the period 2000–2010 showing greater lake growth than during the previous 8 yr since 1992, or 15 yr since 1985. This agrees with our findings of higher glacial decline rates during the 2000s than during the 1990s.

Laguna Sibinacocha (Lake ID: 2, Figs. 9 and 14) illustrates the growth of a lake situated just downstream of a glacial tongue, a lake growth of 12 % in the three decades between 1982 and 2011. This lake appears to have seen the majority of its growth during the mid-late 1990s, which corresponds well with the significant decrease in glacial area during the strong positive El Niño Southern Oscillation (ENSO) event of 1998, which has been suggested to impact glacial behavior in this region (Vuille et al., 2008a; Albert, 2007; Rabatel et al., 2013; Salzmann et al., 2013). At least, the coincidence in timing to other lake-area observations and the increase in glacial melt rates likely point to a regional climatic signal. We also notice the development of many smaller lakes in this region during that time, indicating the likelihood that this area became

TCD

7, 573–634, 2013

Glacial areas, lake areas, and snowlines from 1975 to 2012

M. N. Hanshaw and
B. Bookhagen

Title Page

Abstract

Introduction

Conclusions

References

Tables

Figures

⏪

⏩

◀

▶

Back

Close

Full Screen / Esc

Printer-friendly Version

Interactive Discussion

much wetter. We therefore hypothesize that this lake level change is a combination of enhanced glacial and permafrost melting at high elevation, in addition to more rainfall and precipitation at lower elevation.

The timing of this lake area increase is similar to other lake-area observations (IDs 8 and 33, Figs. 15 and 16, respectively), whose lake areas also began rapidly increasing during the late 1990s. These lakes, however, increased more significantly during the early 2000s. In order to investigate the relationship between glacial decline and lake area increase in more depth, we have generated time series emphasizing the area changes (slopes) for eight proglacial lakes surrounding the QIC (Fig. 17, locations of lakes in Fig. 24). In 2001, glacial area rapidly increased, but then rapidly melted during the subsequent year (2002). This rapid increase in meltwater caused all lakes surrounding the QIC to simultaneously increase, indicating how connected this relationship between glacial melt and proglacial lake growth is.

In order to put our analysis into an expanded spatial context, we show the lake-area trend for all 50 identified lakes (Fig. 23). Using the SRTM DEM, we delineated the watersheds for each of the lakes, and identified whether they were connected to glacial regions or not. The most recent lake area was normalized against the earliest lake area (using Landsat TM images only): values greater than 1 indicate growing regions, values less than 1 are declining.

The majority of declining lakes can be found in watersheds with no connection to glacial meltwaters. Specifically, between the mid-late 1980s and 2011, 84.1 % of lakes not connected to glacial meltwaters have declined. In contrast, 61.3% of lakes connected to glacial meltwaters have increased in area. This suggests again that lakes within glacial watersheds are benefiting from the increased glacial melting that has occurred over the time period of this study. In order to highlight the growth of proglacial lakes, we show glacial-lake area changes for the QIC (Figs. 24 and 17). Most lakes are located on the low-sloping parts of the internally drained Altiplano-Puna Plateau and show moderate or significant growth during the past 25 yr. We note that some proglacial lakes (e.g., Lake IDs 26 and 35) have increased in area initially, but now

Glacial areas, lake areas, and snowlines from 1975 to 2012

M. N. Hanshaw and B. Bookhagen

Title Page

Abstract

Introduction

Conclusions

References

Tables

Figures



Back

Close

Full Screen / Esc

Printer-friendly Version

Interactive Discussion



appear to be decreasing in area, although more data are needed to determine whether this is a pattern or not (Fig. 24).

Reporting specific values for our 50 identified lakes, between 1988 and 2010 (to align with the 1988–2010 glacial area measurements), lakes connected to glacial watersheds increased in area by 12.4%. In contrast, lakes not connected to glacial watersheds decreased in area by 1.9% over the same period. As the trend in glacierized regions has been characterized by significant glacial melting (32% over the same time period), we hypothesize that lakes connected to glacial watersheds, and therefore glacial meltwaters, are increasing as a result of the decline in glacierized areas. In contrast, lakes not connected to glacier watersheds are predominantly stable or declining in area.

However, some drainage basins are characterized by cascading lakes and we observe that some lakes closest to glaciers (i.e., the first or second lakes downstream of a glacier) are growing, whereas lakes further downstream may show an areally stable, or even declining, signal. For example, the north-westerly downstream section of the MGRCV (Glacial ID: 2, Fig. 23).

To summarize, proglacial lakes (e.g., shown in Figs. 14, 15, and 16) are in good spatial and temporal agreement with glacial melting. Several of these lakes are dammed and constrained behind previous glacial moraines and they pose a dangerous natural hazard to vulnerable downstream communities as the water builds behind these moraines. Case studies on such natural hazards including GLOFs have been widely documented in the Cordillera Blanca of Peru (Carey, 2005; Hubbard et al., 2005; Vilímek et al., 2005; Hegglin and Huggel, 2008), north of this study area, but these hazards exist in this region too.

6.3 Snowlines

Very few measurements of snowlines currently exist in this region. Those that do date back to the 1970s and 1980s, with no more recent measurements. The highest altitude the snowline reaches for a given year, as measured on satellite imagery, provides a

Glacial areas, lake areas, and snowlines from 1975 to 2012

M. N. Hanshaw and
B. Bookhagen

Title Page

Abstract

Introduction

Conclusions

References

Tables

Figures

⏪

⏩

◀

▶

Back

Close

Full Screen / Esc

Printer-friendly Version

Interactive Discussion



Glacial areas, lake areas, and snowlines from 1975 to 2012

M. N. Hanshaw and
B. Bookhagen

Title Page

Abstract

Introduction

Conclusions

References

Tables

Figures

⏪

⏩

◀

▶

Back

Close

Full Screen / Esc

Printer-friendly Version

Interactive Discussion

good estimate of the ELA (Rabatel et al., 2012), the altitude at which the zone of accumulation transitions to the zone of ablation. Given the extensive glacier dataset in this study, we have used several images to delineate the snowline for the QIC over the last two decades (Fig. 18). Comparing our measurements to those of previous studies in order to validate our measurements, however, is complicated by the fact that our images usable for snowline analysis did not date back to those of the previous measurements. Additionally, the earlier measurements provide lower elevations for the snowline, as can be seen in Fig. 18. Given that previous studies report slow retreat during the 20 yr of the 1970s and 1980s, our slightly higher snowline elevations of the late 1980s are not unreasonable following this pattern. Additionally, when performing comparisons it is difficult, if not impossible, to determine how previous studies have measured the snowline (i.e., on what date, on what point of the glacier, whether it is a mean measurement, as the snowline is rarely consistent around the glacier, or a maximum measurement etc.). Additionally, most elevation measurements likely have some uncertainty associated with them, and this uncertainty will be large at these altitudes. The measurements presented in this study have been created by a consistent method and the relative patterns should be accurate due to this consistency.

During the 1990s, glacial retreat occurred more rapidly than during the previous decade and is reflected by the snowline changes. Snowlines increased to higher elevations, particularly during 1998, which saw the highest snowline altitude throughout the study period. We note again that 1998 corresponds to a strong positive ENSO event, and we also observed lower-than-average glacial-area measurements during this year (Figs. 10, 11, and 12) that are synchronous with snowline-elevation increases. Subsequently, during the 2000s, the transient snowline has advanced again to lower altitudes, yet increasing again during positive ENSO of 2009. Interestingly, 2009 also indicates the lowest measured areas of our glacierized regions over the time period of this study (Figs. 10, 11, and 12).

7 Conclusions

This study makes use of a multitude of multi-spectral satellite images to obtain time series of glacial and lake areas throughout the Cordillera Vilcanota (CV) in the northern central Andes from 1975 to 2012. In addition, we investigated snowlines for the Quelccaya Ice Cap (QIC).

Our results indicate that glacierized areas have declined throughout the CV, by an average of 32 % since 1988. Smaller glacierized areas have, in general, higher decline rates than those of larger glacierized areas, however, the trends in decline rates are similar for glacierized areas of all sizes: decline rates have been significantly higher during the most recent decade (2000–2011) than during the previous decade (1990–2000). Glacierized regions at lower elevations are also retreating to higher elevations faster than those already at higher elevations. Snowline elevation results for the QIC reflect area measurements for the entire QIC: the snowline is gradually retreating to higher altitudes as the QIC shrinks in size. The positive ENSO years of 1998/1999 and 2009/2010 appear to have caused rapid snowline retreat and also significant declines in glacial area. When comparing different studies, we emphasize the importance of including the image date: our data for the QIC indicates that in the most extreme case of our time series, area measurements can vary by up to 19 % within the dry ablation season of a single year.

The retreat of glacierized regions throughout the CV and beyond has provided increased meltwaters to the downstream lakes of the region. Proglacial lakes have either grown or were formed since the beginning of our study's time series. The majority of proglacial lake growth has occurred since the mid-late 1990s, which corresponds well with the increase in glacial decline rates. In the case of proglacial lakes surrounding the QIC, the main lake-area increase occurred during 2002, coeval with a significant decline in glacial area the previous year. Spatially, it is evident that the majority of lakes downstream of glacial watersheds are growing, while those lakes not downstream of glacial watersheds are mostly remaining stable or declining.

Glacial areas, lake areas, and snowlines from 1975 to 2012

M. N. Hanshaw and
B. Bookhagen

Title Page

Abstract

Introduction

Conclusions

References

Tables

Figures

◀

▶

◀

▶

Back

Close

Full Screen / Esc

Printer-friendly Version

Interactive Discussion

spaceborne imagery, *Nat. Hazards Earth Syst. Sci.*, 8, 1329–1340, doi:10.5194/nhess-8-1329-2008, 2008.

Bookhagen, B. and Burbank, D. W.: Toward a complete Himalayan hydrological budget: Spatiotemporal distribution of snowmelt and rainfall and their impact on river discharge, *J. Geophys. Res.*, 115, F03019, doi:10.1029/2009JF001426, 2010.

Bookhagen, B. and Strecker, M. R.: Orographic barriers, high-resolution TRMM rainfall, and relief variations along the eastern Andes, *Geophys. Res. Lett.*, 35, 1–6, 2008.

Bradley, R., Vuille, M., Diaz, H. and Vergara, W.: Threats to water supplies in the tropical Andes, *Science*, 312, 1755–1756, 2006.

Brecher, H. H. and Thompson, L. G.: Measurement of the retreat of Qori Kalis glacier in the Tropical Andes of Peru by Terrestrial Photogrammetry, *Photogramm. Eng. Rem. S.*, 59, 1017–1022, 1993.

Bronge, L. and Bronge, C.: Ice and snow-type classification in the Vestfold Hills, East Antarctica, using Landsat-TM data and ground radiometer measurements, *Int. J. Remote Sens.*, 20, 225–240, 1999.

Carey, M.: Living and dying with glaciers: people's historical vulnerability to avalanches and outburst floods in Peru, *Global Planet. Change*, 47, 122–134, 2005.

Chan, J., Van Ophem, J., and Huybrechts, P.: Estimation of accumulation area ratio of a glacier from multi-temporal satellite images using spectral unmixing, *Geoscience and Remote Sensing Symposium, IEEE*, 2, 606–609, 2009.

Clare, G. R., Fitzharris, B. B., Chinn, T. J. H., and Salinger, M. J.: Interannual variation in end-of-summer snowlines of the Southern Alps of New Zealand, and relationships with Southern Hemisphere atmospheric circulation and sea surface temperature patterns, *Int. J. Climatol.*, 22, 107–120, 2002.

Farr, T., Rosen, P., Caro, E., Crippen, R., Duren, R., Hensley, S., Kobrick, M., Paller, M., Rodriguez, E., Roth, L., Seal, D., Shaffer, S., Shimada, J., Umland, J., Werner, M., Oskin, M., Burbank, D., and Alsdorf, D.: The Shuttle Radar Topography Mission, *Rev. Geophys.*, 45, RG2004, doi: 10.1029/2005RG000183, 2007.

Gardelle, J., Arnaud, Y., and Berthier, E.: Contrasted evolution of glacial lakes along the Hindu Kush Himalaya mountain range between 1990 and 2009, *Global Planet. Change*, 75, 47–55, 2011.

Georges, C.: 20th-Century Glacier Fluctuations in the Tropical Cordillera Blanca, Peru, *Arct. Antarct. Alp. Res.*, 36, 100–107, 2004.

Glacial areas, lake areas, and snowlines from 1975 to 2012

M. N. Hanshaw and
B. Bookhagen

Title Page

Abstract

Introduction

Conclusions

References

Tables

Figures

⏪

⏩

◀

▶

Back

Close

Full Screen / Esc

Printer-friendly Version

Interactive Discussion

- Hall, D., Ormsby, J., Bindschadler, R., and Siddalingaiah, H.: Characterization of snow and ice reflectance zones on glaciers using Landsat Thematic Mapper data, *Ann. Glaciol.*, 9, 104–108, 1987.
- Hastenrath, S.: Heat-budget measurements on the Quelccaya Ice Cap, Peruvian Andes, *J. Glaciol.*, 20, 85–97, 1978.
- Hastenrath, S.: Cordillera Blanca on Landsat imagery and Quelccaya Ice Cap, in: *Satellite Image Atlas of the World – South America*, edited by: Williams, R. and Ferrigno, J., USGS Professional Paper 1386-I, 1998.
- Hegglin, E. and Huggel, C.: An Integrated Assessment of Vulnerability to Glacial Hazards, *Mt. Res. Dev.*, 28, 299–309, 2008.
- Hidrandina, S. A.: *Glacier Inventory of Perú*, Consejo Nacional de Ciencia y Tecnología, Perú, 1988.
- Hubbard, B., Heald, A., Reynolds, J. M., Quincey, D., Richardson, S. D., Luyo, M. Z., Portilla, N. S., and Hambrey, M. J.: Impact of a rock avalanche on a moraine-dammed proglacial lake: Laguna Safuna Alta, Cordillera Blanca, Peru, *Earth Surf. Proc. Land.*, 30, 1251–1264, 2005.
- Huggel, C., Kääb, A., Haeberli, W., Teyssere, P., and Paul, F.: Remote sensing based assessment of hazards from glacier lake outbursts: a case study in the Swiss Alps, *Can. Geotech. J.*, 330, 316–330, 2002.
- Huggel, C., Salzmann, N., Allen, S., Caplan-Auerbach, J., Fischer, L., Haeberli, W., Larsen, C., Schneider, D., and Wessels, R.: Recent and future warm extreme events and high-mountain slope stability, *Philos. T. R. Soc. A*, 368, 2435–2459, 2010.
- IPCC: *Climate Change 2007: The Physical Science Basis*, in: *Contribution of Working Group I to the Fourth Assessment Report of the Intergovernmental Panel on Climate Change*, edited by: Solomon, S., Qin, D., Manning, M., Chen, Z., Marquis, M., Averyt, K. B., Tignor, M., and Miller, H. L., Cambridge University Press, Cambridge, United Kingdom and New York, NY, USA, 2007.
- Kaser, G. and Georges, C.: Changes of the equilibrium-line altitude in the tropical Cordillera Blanca, Peru, 1930–50, and their spatial variations, *Ann. Glaciol.*, 24, 344–349, 1997.
- Kaser, G. and Georges, C.: On the mass balance of low latitude glaciers with particular consideration of the Peruvian Cordillera Blanca, *Geogr. Ann. A*, 81, 643–651, 1999.
- Kaser, G., Großhauser, M., and Marzeion, B.: Contribution potential of glaciers to water availability in different climate regimes, *P. Natl. Acad. Sci. USA*, 107, 20223–20227, 2010.

Glacial areas, lake areas, and snowlines from 1975 to 2012

M. N. Hanshaw and
B. Bookhagen

[Title Page](#)[Abstract](#)[Introduction](#)[Conclusions](#)[References](#)[Tables](#)[Figures](#)[⏪](#)[⏩](#)[◀](#)[▶](#)[Back](#)[Close](#)[Full Screen / Esc](#)[Printer-friendly Version](#)[Interactive Discussion](#)

Klein, A. G. and Isacks, B. L.: Spectral mixture analysis of Landsat thematic mapper images applied to the detection of the transient snowline on tropical Andean glaciers, *Global Planet. Change*, 22, 139–154, 1999.

Mark, B. G., Seltzer, G. O., Rodbell, D. T., and Goodman, A. Y.: Rates of Deglaciation during the Last Glaciation and Holocene in the Cordillera Vilcanota-Queelccaya Ice Cap Region, Southeastern Perú, *Quaternary Res.*, 57, 287–298, 2002.

Masek, J., Honzak, M., Goward, S., Liu, P., and Pak, E.: Landsat-7 ETM+ as an observatory for land cover: Initial radiometric and geometric comparisons with Landsat-5 Thematic Mapper, *Remote Sens. Environ.*, 78, 118–130, 2001.

Mathieu, R., Chinn, T., and Fitzharris, B.: Detecting the equilibrium-line altitudes of New Zealand glaciers using ASTER satellite images, *New Zeal. J. Geol. Geop.*, 52, 209–222, 2009.

Mercer, J. H. and Palacios, O. M.: Radiocarbon dating of the last glaciation in Perú, *Geology*, 5, 600–604, 1977.

Morales Arnao, B.: Glaciers of Peru, in: *Satellite Image Atlas of the World – South America*, edited by: Williams, R. and Ferrigno, J., USGS Professional Paper, 1386-I, 1998.

Østrem, G.: ERTS data in glaciology – an effort to monitor glacier mass balance from satellite imagery, *J. Glaciol.*, 15, 403–415, 1975.

Painter, T., Roberts, D., Green, R., and Dozier, J.: The effect of grain size on spectral mixture analysis of snow-covered area from AVIRIS data, *Remote Sens. Environ.*, 65, 320–332, 1998.

Paul, F. and Kääb, A.: Perspectives on the production of a glacier inventory from multispectral satellite data in Arctic Canada: Cumberland Peninsula, Baffin Island, *Ann. Glaciol.*, 42, 59–66, 2005.

Paul, F., Barry, R., Cogley, J., Frey, H., Haeberli, W., Ohmura, A., Ommanney, C., Raup, B., Rivera, A., and Zemp, M.: Recommendations for the compilation of glacier inventory data from digital sources, *Ann. Glaciol.*, 50, 119–126, 2009.

Rabatel, A., Dedieu, J. and Vincent, C.: Using remote-sensing data to determine equilibrium-line altitude and mass-balance time series: validation on three French glaciers, 1994–2002, *J. Glaciol.*, 51, 539–546, 2005.

Rabatel, A., Bermejo, A., Loarte, E., Soruco, A., Gomez, J., Leonardini, G., Vincent, C., and Sicart, J. E.: Can the snowline be used as an indicator of the equilibrium line and mass balance for glaciers in the outer tropics?, *J. Glaciol.*, 58, 1027–1036, 2012.

Glacial areas, lake areas, and snowlines from 1975 to 2012

M. N. Hanshaw and
B. Bookhagen

[Title Page](#)[Abstract](#)[Introduction](#)[Conclusions](#)[References](#)[Tables](#)[Figures](#)[⏪](#)[⏩](#)[◀](#)[▶](#)[Back](#)[Close](#)[Full Screen / Esc](#)[Printer-friendly Version](#)[Interactive Discussion](#)

- Rabatel, A., Francou, B., Soruco, A., Gomez, J., Cáceres, B., Ceballos, J. L., Basantes, R., Vuille, M., Sicart, J.-E., Huggel, C., Scheel, M., Lejeune, Y., Arnaud, Y., Collet, M., Condom, T., Consoli, G., Favier, V., Jomelli, V., Galarraga, R., Ginot, P., Maisincho, L., Mendoza, J., Ménégos, M., Ramirez, E., Ribstein, P., Suarez, W., Villacis, M., and Wagnon, P.: Current state of glaciers in the tropical Andes: a multi-century perspective on glacier evolution and climate change, *The Cryosphere*, 7, 81–102, doi:10.5194/tc-7-81-2013, 2013.
- Racoviteanu, A. E., Arnaud, Y., Williams, M. W. and Ordoñez, J.: Decadal changes in glacier parameters in the Cordillera Blanca, Peru, derived from remote sensing, *J. Glaciol.*, 54, 499–510, 2008a.
- Racoviteanu, A. E., Williams, M. W., and Barry, R. G.: Optical Remote Sensing of Glacier Characteristics: A Review with Focus on the Himalaya, *Sensors*, 8, 3355–3383, 2008b.
- Racoviteanu, A., Paul, F., Raup, B., Khalsa, S. J. S., and Armstrong, R.: Challenges and recommendations in mapping of glacier parameters from space: results of the 2008 Global Land Ice Measurements from Space (GLIMS) workshop, Boulder, Colorado, USA, *Ann. Glaciol.*, 50, 53–69, 2009.
- Roberts, D., Gardner, M., Church, R., Ustin, S., Scheer, G., and Green, R.: Mapping Chaparral in the Santa Monica Mountains using Multiple Endmember Spectral Mixture Models, *Remote Sens. Environ.*, 65, 267–279, 1998.
- Roberts, D., Halligan, K., and Dennison, P.: VIPER Tools User Manual, UC Santa Barbara, Department of Geography, Version 1.7, 1–91, 2007.
- Salzmann, N., Huggel, C., Rohrer, M., Silverio, W., Mark, B. G., Burns, P., and Portocarrero, C.: Glacier changes and climate trends derived from multiple sources in the data scarce Cordillera Vilcanota region, southern Peruvian Andes, *The Cryosphere*, 7, 103–118, doi:10.5194/tc-7-103-2013, 2013.
- Silverio, W. and Jaquet, J.: Glacial cover mapping (1987–1996) of the Cordillera Blanca (Peru) using satellite imagery, *Remote Sens. Environ.*, 95, 342–350, 2005.
- Soruco, A., Vincent, C., Francou, B., and Gonzalez, J. F.: Glacier decline between 1963 and 2006 in the Cordillera Real, Bolivia, *Geophys. Res. Lett.*, 36, 2–7, 2009.
- Surazakov, A. and Aizen, V.: Positional accuracy evaluation of declassified Hexagon KH-9 mapping camera imagery, *Camera*, 76, 603–608, 2010.
- Svoboda, F. and Paul, F.: A new glacier inventory on southern Baffin Island, Canada, from ASTER data: I. Applied methods, challenges and solutions, *Ann. Glaciol.*, 50, 11–21, 2009.

Glacial areas, lake areas, and snowlines from 1975 to 2012M. N. Hanshaw and
B. Bookhagen[Title Page](#)[Abstract](#)[Introduction](#)[Conclusions](#)[References](#)[Tables](#)[Figures](#)[⏪](#)[⏩](#)[◀](#)[▶](#)[Back](#)[Close](#)[Full Screen / Esc](#)[Printer-friendly Version](#)[Interactive Discussion](#)

Thompson, L.: Glaciological investigations of the tropical Quelccaya ice cap, Peru, *J. Glaciol.*, 25, 69–84, 1980.

Thompson, L. G., Hastenrath, S., and Arnao, B. M.: Climatic Ice Core Records from the Tropical Quelccaya Ice Cap, *Science*, 203, 1240–1243, 1979.

5 Thompson, L., Mosley-Thompson, E., Bolzan, J., and Koci, B.: A 1500-Year Record of Tropical Precipitation in Ice Cores from the Quelccaya Ice Cap, Peru, *Science*, 229, 971–973, 1985.

Thompson, L. G., Mosley-Thompson, E., Brecher, H., Davis, M., León, B., Les, D., Lin, P.-N., Mashiotto, T., and Mountain, K.: Abrupt tropical climate change: past and present, *P. Natl. Acad. Sci. USA*, 103, 10536–10543, 2006.

10 Vergara, W., Deeb, A. M., Valencia, A. M., Bradley, R. S., Francou, B., Zarzar, A., Grünwaldt, A., and Haeussling, S. M.: Economic Impacts of Rapid Glacier Retreat in the Andes, *EOS Transactions, American Geophysical Union*, 88, 261, 2007.

Vilímek, V., Zapata, M. L., Klimeš, J., Patzelt, Z., and Santillán, N.: Influence of glacial retreat on natural hazards of the Palcacocha Lake area, Peru, *Landslides*, 2, 107–115, 2005.

15 Vuille, M., Francou, B., Wagnon, P., Juen, I., Kaser, G., Mark, B., and Bradley, R. S.: Climate change and tropical Andean glaciers: Past, present and future, *Earth-Sci. Rev.*, 89, 79–96, 2008a.

Vuille, M., Kaser, G., and Juen, I.: Glacier mass balance variability in the Cordillera Blanca, Peru and its relationship with climate and the large-scale circulation, *Global Planet. Change*, 62, 14–28, 2008b.

20 Wessels, R. L., Kargel, J. S., and Kieffer, H. H.: ASTER measurement of supraglacial lakes in the Mount Everest region of the Himalaya, *Ann. Glaciol.*, 34, 399–408, 2002.

WGMS and NSIDC: World Glacier Inventory, Compiled and made available by the World Glacier Monitoring Service, Zurich, Switzerland, and the National Snow and Ice Data Center, Boulder CO, USA Digital Media, 1989, updated 2009.

25 Yu, J., Liu, H., Wang, L., Jezek, K. C., and Heo, J.: Blue ice areas and their topographical properties in the Lambert glacier, Amery Iceshelf system using Landsat ETM+, ICESat laser altimetry and ASTER GDEM data, *Antarct. Sci.*, 24, 95–110, 2012.

Glacial areas, lake areas, and snowlines from 1975 to 2012

M. N. Hanshaw and
B. Bookhagen

Title Page

Abstract

Introduction

Conclusions

References

Tables

Figures

⏪

⏩

◀

▶

Back

Close

Full Screen / Esc

Printer-friendly Version

Interactive Discussion



Table 1. Characteristics of the satellites and sensors used in this study. Bands in italics are those that have not been used. Data sources are as follows: Corona (Surazakov and Aizen, 2010), Landsat (<http://landsat.gsfc.nasa.gov/about/technical.html>), ASTER (<http://asterweb.jpl.nasa.gov>). Table modified after Svoboda and Paul (2009).

	Corona KH-9	Landsat MSS (1–3)	Landsat MSS (4–5)	Landsat TM	Landsat ETM+	ASTER
Date Range of Images Used	1980	1975	1982–1985	1985–2011	1999–2003	2001–2012
No. of Images: Total (& Lakes)	1	3	3	96	6	35
No. of Images: Glaciers	1	2	1	56	4	13
Path/Row of Images Used	Mission 1216	002-003/070	003/070	003/070	003/070	multiple
Band: Wavelengths (μm)	–	–	–	1: 0.45–0.52	1: 0.45–0.52	–
Visible:	Unknown	4: 0.5–0.6 5: <i>0.6–0.7</i>	1: 0.5–0.6 2: <i>0.6–0.7</i>	2: 0.52–0.60 3: 0.63–0.69	2: 0.52–0.60 3: 0.63–0.69	1: 0.52–0.60 2: <i>0.63–0.69</i>
Near IR:	–	6: 0.7–0.8 7: 0.8–1.1	3: <i>0.7–0.8</i> 4: 0.8–1.1	4: 0.76–0.90	8: 0.52–0.90 (VNIR panchro.) 4: 0.77–0.90	3N/B: 0.76–0.86 (Nadir & Back)
Short-Wave IR:	–	–	–	5: 1.55–1.75 7: 2.08–2.35	5: 1.55–1.75 7: 2.08–2.35	4: 1.60–1.70 5–9: 2.145–2.430 (5 bands)
Thermal IR:	–	–	–	6: <i>10.40–12.50</i>	6: <i>10.40–12.50</i>	10–14: <i>8.125–11.65 (5 bands)</i>
Spatial Resolution (m)	6–9 m	68 × 83 *	68 × 83 *	1–5 & 7: 30 6: 120	1–5 & 7: 30 6: 60 8: 15	1–3: 15 m 4–9: 30 10–14: 90
Image Size (km)	250 × 125	185 × 185	185 × 185	~ 170 × 183	~ 170 × 183	~ 60 × 60
Temporal Resolution (days)	–	18	16	16	16	16
Orbit	–	polar, sun-synchronous	polar, sun-synchronous	polar, sun-synchronous	polar, sun-synchronous	polar, sun-synchronous
Altitude (km)	171	900	900	705	705	705
Inclination (°)	96.5	99.2	99.2	98.2	98.2	98.3
Comments		* commonly resampled to 60 m	* commonly resampled to 60 m	Stopped acquiring images in November 2011	Scan Line Corrector failure in May 2003	SWIR failure (anomalous saturation) in May 2007

Glacial areas, lake areas, and snowlines from 1975 to 2012

M. N. Hanshaw and
B. Bookhagen

Table 2. Summary of methods and thresholds used in lake and glacier classifications. The threshold for shadows in the hillshades (HS) was DN < 70 for all images. DN represents digital number, CF and MF with their kernel sizes stand for closing filter and median filter, respectively.

Sensor	Method	Lakes			Filtering	Method	Glaciers	
		Threshold (Mean, Median, Mode)					Threshold	Filtering
Corona	Manual	–	–	–	–	Manual	–	–
Landsat MSS (1–3)	(MSS7-MSS4)/(MSS7 + MSS4) and HS	< -0.17	< -0.25	< -0.25	CF-5 × 5	Density Slice	DN 105–255 (MSS6)	MF-3 × 3
Landsat MSS (4–5)	(MSS4-MSS1)/(MSS4 + MSS1) and HS	< -0.08	< 0.00	< 0.00	CF-5 × 5	Density Slice	DN 165-255 (MSS1)	MF-3 × 3
Landsat TM	NDWI and HS	< -0.51	< -0.50	< -0.50	CF-5 × 5	TM3/TM5 & TM1	≥ 2.0 & > 25	MF-3 × 3 & CF-5 × 5
Landsat ETM+	NDWI and HS	< -0.40	< -0.40	< -0.40	CF-5 × 5	ETM3/ETM5 & ETM1	≥ 2.0 & > 25	MF-3 × 3 & CF-5 × 5
ASTER (w/ SWIR)	(AST3-AST1)/(AST3 + AST1) or AST 3 and HS	< -0.24	< -0.25	< -0.25	CF-3 × 3	AST3/AST4 & AST1	≥ 1.6 & > 47	MF-3 × 3
ASTER (w/o SWIR)	(AST3-AST1)/(AST3+AST1) or AST 3 and HS	< -0.24	< -0.25	< -0.25	CF-3 × 3	Manual	–	–
		OR ≤ 1000	OR ≤ 1000	OR ≤ 1000				

[Title Page](#)
[Abstract](#) [Introduction](#)
[Conclusions](#) [References](#)
[Tables](#) [Figures](#)
⏪ ⏩
◀ ▶
[Back](#) [Close](#)
[Full Screen / Esc](#)
[Printer-friendly Version](#)
[Interactive Discussion](#)



Glacial areas, lake areas, and snowlines from 1975 to 2012

M. N. Hanshaw and
B. Bookhagen

Table 4. Additional information corresponding to Fig. 13, normalized decline rates for each Glacial ID.

Glacier ID	198X–2011				1990–2000				2000–2011			
	No. of data points	RMSE ($\text{km}^2 \text{yr}^{-1} \text{km}^{-2}$)	Median area (km^2)	Median elevation (m a.s.l.)	No. of data points	RMSE ($\text{km}^2 \text{yr}^{-1} \text{km}^{-2}$)	Median area (km^2)	Median elevation (m a.s.l.)	No. of data points	RMSE ($\text{km}^2 \text{yr}^{-1} \text{km}^{-2}$)	Median area (km^2)	Median elevation (m a.s.l.)
7 (NCt)	24	0.14	2.5	5276	10	0.07	2.9	5272	11	0.13	2.1	5288
9 (NCc)	22	0.24	2.5	5241	9	0.25	2.9	5238	11	0.24	2.2	5253
10 (NM)	21	0.82	2.9	5236	9	0.88	3.2	5234	11	0.59	2.4	5247
4 (NI)	20	0.37	4.9	5070	8	0.08	5.9	5065	10	0.32	4.5	5084
6 (NS)	19	0.18	9.5	5055	8	0.05	11.0	5051	10	0.26	7.6	5075
5 (NP)	24	0.68	10.6	5278	10	0.59	11.4	5274	12	0.83	6.6	5343
8 (NAc)	16	0.11	22.8	5192	6	0.08	26.0	5177	9	0.14	20.0	5212
3 (NA)	21	0.09	32.0	5253	9	0.05	33.6	5244	10	0.08	30.5	5276
1 (QIC)	24	0.07	53.2	5407	9	0.05	55.7	5395	12	0.08	47.9	5420
2 (MGRCV)	19	0.15	206.9	5324	8	0.10	217.1	5311	9	0.10	189.1	5339

↑
increasing area
↓

Title Page

Abstract

Introduction

Conclusions

References

Tables

Figures

⏪

⏩

◀

▶

Back

Close

Full Screen / Esc

Printer-friendly Version

Interactive Discussion

Glacial areas, lake areas, and snowlines from 1975 to 2012

M. N. Hanshaw and
B. Bookhagen

Title Page

Abstract

Introduction

Conclusions

References

Tables

Figures

⏪

⏩

◀

▶

Back

Close

Full Screen / Esc

Printer-friendly Version

Interactive Discussion

Table 5. Area measurements of the QIC from both this study and other studies. *Entire* QIC refers to all snow-covered regions identified in the earliest image, while *Main* QIC refers to a subset of this, the largest continuous ice mass (cf. Fig. 19). Our study has included the entire QIC area, i.e., all ice- and snow-covered regions that lie within the area of the earliest image (28 October 1975, Fig. 19a), and has captured smaller ice areas outside of the main QIC area.

Year	This study		Other studies		Source	
	Imagery	Area in km ²		Area in km ²		
		<i>Entire</i> QIC	<i>Main</i> QIC	<i>Entire</i> QIC (Assumed)		<i>Main</i> QIC (Assumed)
1962				56.3	Ames et al. (1989)	
1975	Landsat MSS 2	81.7	77.7	58.9	Albert (2007)	
1980	Corona KH-9	63.1	56.8	56.2	Salzmann et al. (2013)	
1985	Landsat TM	71.3	62.4	55.0	Thompson (1980)	
				70.0	Mark et al. (2002)	
				58.0	Albert (2002)	
1991	Landsat TM	58.7	53.2	55.7	Salzmann et al. (2013)	
				50.9	Albert (2007)	
1998	Landsat TM	51.3	47.7	47.9	Salzmann et al. (2013)	
2000	Landsat TM	52.1	47.5	47.3	Albert (2007)	
				47.0	Albert (2007)	
				45.9	Salzmann et al. (2013)	
2006	Landsat TM	47.8	44.4	44.2	Salzmann et al. (2013)	
2009	Landsat TM	43.7	41.8	42.8	Salzmann et al. (2013)	

Glacial areas, lake areas, and snowlines from 1975 to 2012

M. N. Hanshaw and
B. Bookhagen

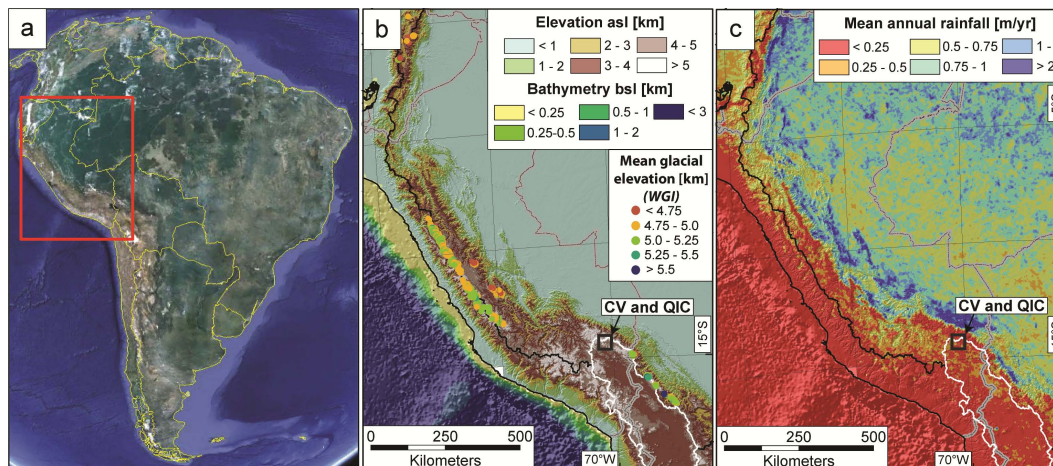


Fig. 1. Location of the study area – (a) South American continent, (b) topography and (c) rainfall for the northern and central Andes. Red rectangle in (a) indicates the area covered in (b) and (c). Included in (b) are some tropical glaciers (colored according to mean glacial elevation) from the World Glacier Inventory (WGMS and NSIDC, 1989), and in (b) and (c) the Amazon drainage basin is denoted by the thin black line, and the northern part of the internally-drained Altiplano-Puna Plateau is displayed by a white line. Topography (b) is derived from the Shuttle Radar Topography Mission (SRTM) DEM, and mean annual rainfall (c) is based on satellite-derived estimates using Tropical Rainfall Measurement Mission (TRMM) product 2B31 averaged from 1998–2010 (Bookhagen and Strecker, 2008; Bookhagen and Burbank, 2010). The small black rectangle in (b) and (c) indicates the more specific study area of the Cordillera Vilcanota (CV) and the Quelccaya Ice Cap (QIC). Note the lack of glacier measurements from the World Glacier Inventory (WGI) in this region. Image in (a) courtesy of Google Earth.

[Title Page](#)
[Abstract](#)
[Introduction](#)
[Conclusions](#)
[References](#)
[Tables](#)
[Figures](#)
[◀](#)
[▶](#)
[◀](#)
[▶](#)
[Back](#)
[Close](#)
[Full Screen / Esc](#)
[Printer-friendly Version](#)
[Interactive Discussion](#)

Glacial areas, lake areas, and snowlines from 1975 to 2012

M. N. Hanshaw and
B. Bookhagen

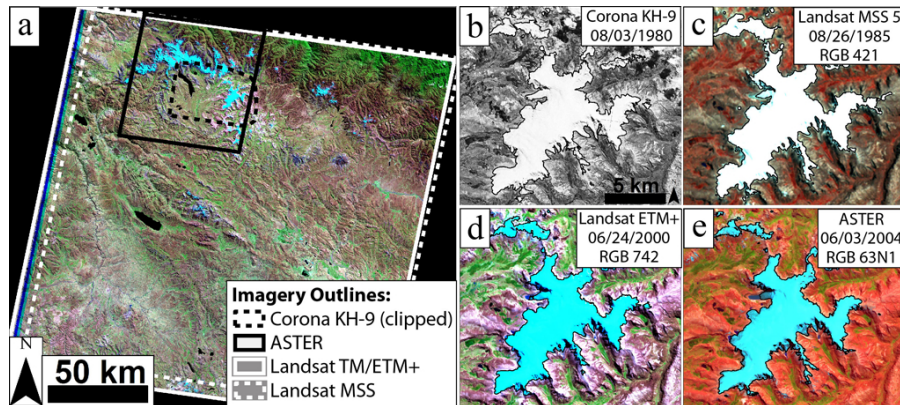


Fig. 2. Overview of imagery used in this study (see Fig. 1 for location). **(a)** Landsat ETM+ image from 24 June 2000 showing Bands 742 RGB with the outlines of the other imagery coverage areas. The QIC is shown in panels **(b–e)** to illustrate the various types of imagery. The black line outlines the QIC extent in each image. Note the areal extent changes between 1980 and 2004.

Title Page

Abstract

Introduction

Conclusions

References

Tables

Figures

◀

▶

◀

▶

Back

Close

Full Screen / Esc

Printer-friendly Version

Interactive Discussion

Glacial areas, lake areas, and snowlines from 1975 to 2012

M. N. Hanshaw and
B. Bookhagen

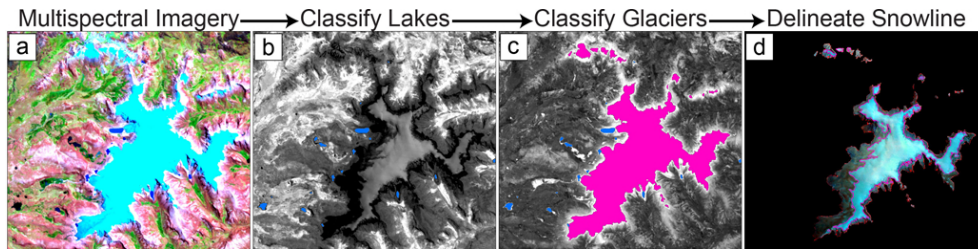


Fig. 3. Flow chart indicating the general methodology used, applied to a Landsat TM image from 16 September 2010. The images **(a)** are used to classify lakes **(b)** using a Normalized Difference Water Index (NDWI) algorithm (lakes: blue). Glaciers **(c)** are then classified using a TM3/TM5 & TM1 algorithm (Landsat TM/ETM+) and clipping of the data with the previously created lake mask to remove incorrectly classified lakes (shown on TM3/TM5 image – lakes: blue, QIC: pink). The QIC (or other glacier) outline is then used to clip calibrated reflectance data **(d)** to obtain snowline information for that area alone using MESMA. See text for abbreviation explanations.

Title Page

Abstract

Introduction

Conclusions

References

Tables

Figures

◀

▶

◀

▶

Back

Close

Full Screen / Esc

Printer-friendly Version

Interactive Discussion

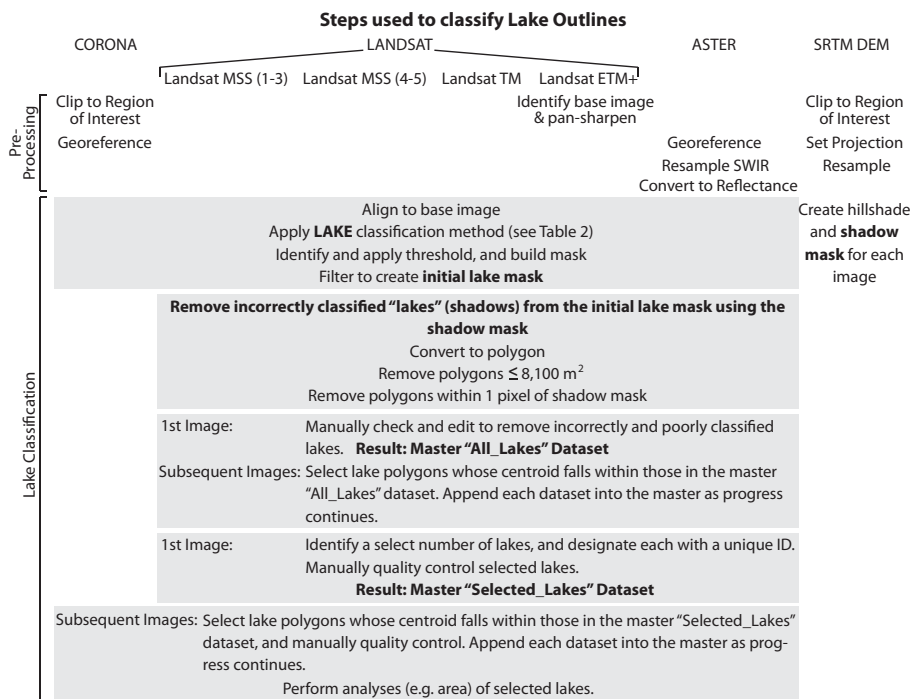


Fig. 4. Steps summarizing the processes used to classify lake outlines, including pre-processing steps. Grey background overlaps those data sets to which each process applies, and bold text indicates important steps or datasets (either complete, or to be used in subsequent processing).

Title Page

Abstract Introduction

Conclusions References

Tables Figures

⏪ ⏩

⏴ ⏵

Back Close

Full Screen / Esc

Printer-friendly Version

Interactive Discussion



Glacial areas, lake areas, and snowlines from 1975 to 2012

M. N. Hanshaw and
B. Bookhagen

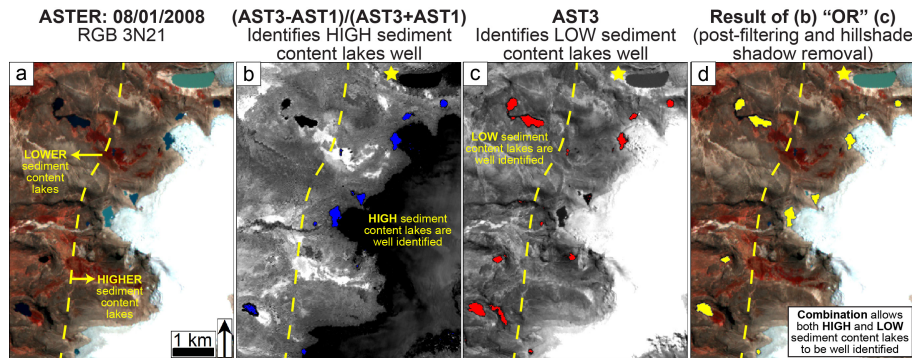


Fig. 5. ASTER image illustrating how lakes of both high and low sediment concentrations were classified in this study. **(a)** highlights part of the QIC where lakes of differing sediment contents exist, **(b)** shows the results of the $(AST3-AST1)/(AST3+AST1)$ ratio (blue pixels: < -0.25), **(c)** shows ASTER B3 (red pixels: ≤ 1000), and **(d)** illustrates the final result when a combination of both methods are used. Note that none of these methods provide a perfect classification, and some lakes remain unidentified (the yellow star indicates the proglacial lake of Qori Kalis glacier and is unclassified using all 3 methods). Yellow dashed line indicates the approximate line of separation between higher and lower sediment content lakes, which is roughly related to distance from the QIC.

Title Page

Abstract Introduction

Conclusions References

Tables Figures

⏪ ⏩

⏴ ⏵

Back Close

Full Screen / Esc

Printer-friendly Version

Interactive Discussion

Glacial areas, lake areas, and snowlines from 1975 to 2012

M. N. Hanshaw and
B. Bookhagen

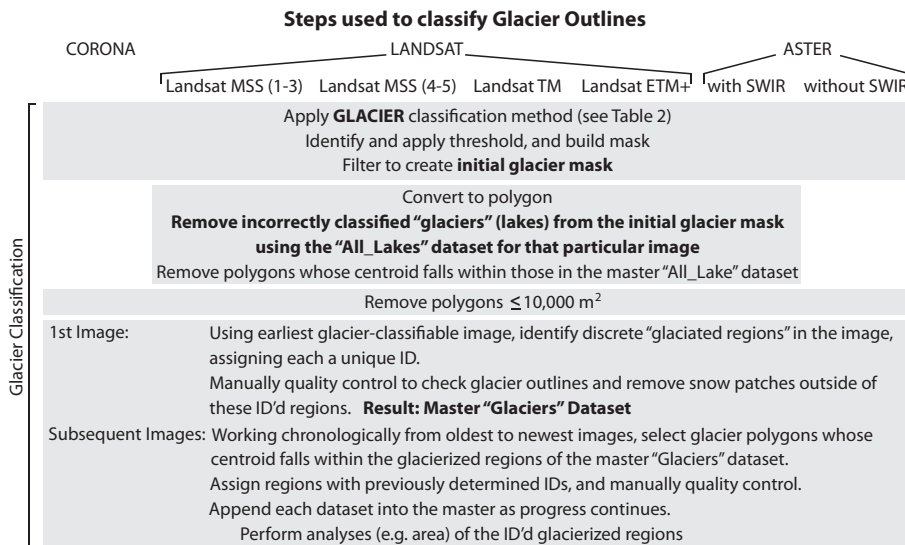


Fig. 6. Steps summarizing the processes used to classify glacial outlines. As with Fig. 4, grey background overlaps those datasets to which each process applies, and bold text indicates important steps or datasets.

Title Page

Abstract Introduction

Conclusions References

Tables Figures

⏪ ⏩

⏴ ⏵

Back Close

Full Screen / Esc

Printer-friendly Version

Interactive Discussion



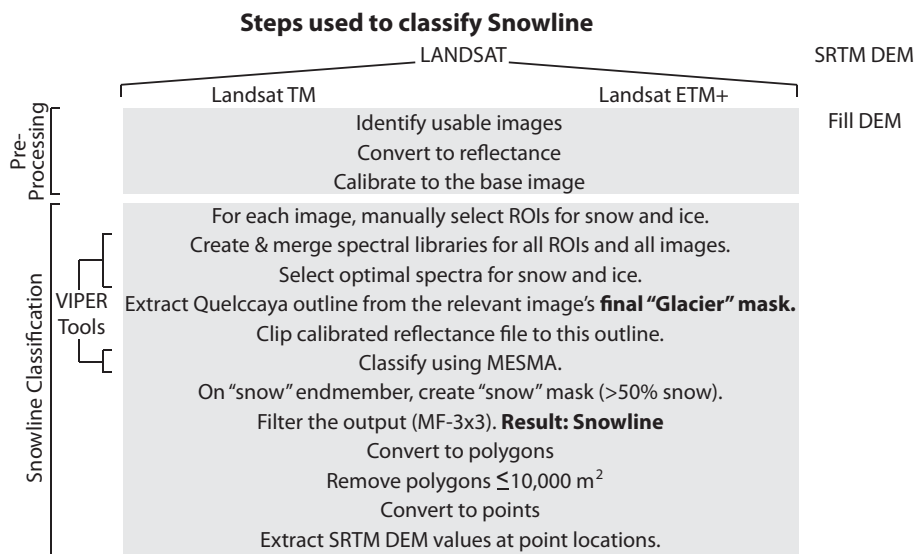


Fig. 7. Steps summarizing the processes used to classify glacier snowlines (specifically the QIC in this study). As with Figs. 4 and 6, grey background overlaps those datasets to which each process applies, and bold text indicates important steps or datasets.

Title Page

Abstract Introduction

Conclusions References

Tables Figures

⏪ ⏩

◀ ▶

Back Close

Full Screen / Esc

Printer-friendly Version

Interactive Discussion

Glacial areas, lake areas, and snowlines from 1975 to 2012

M. N. Hanshaw and
B. Bookhagen

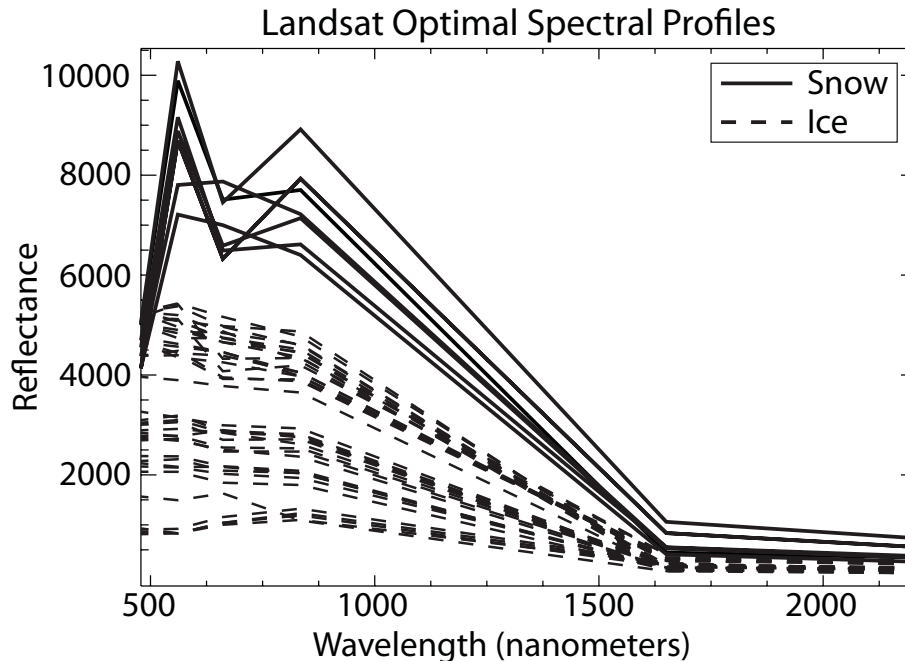


Fig. 8. Optimal spectra used in MESMA analysis for Landsat imagery (17 images ranging from 2 August 1988–16 September 2010). Solid lines indicate snow spectra, and dashed lines indicate ice spectra. Note that there is a general greater variability within the ice spectra than in the snow spectra and we have thus relied on more endmembers for ice.

[Title Page](#)
[Abstract](#)
[Introduction](#)
[Conclusions](#)
[References](#)
[Tables](#)
[Figures](#)
[◀](#)
[▶](#)
[◀](#)
[▶](#)
[Back](#)
[Close](#)
[Full Screen / Esc](#)
[Printer-friendly Version](#)
[Interactive Discussion](#)

Glacial areas, lake areas, and snowlines from 1975 to 2012

M. N. Hanshaw and B. Bookhagen

Discussion Paper | Discussion Paper | Discussion Paper | Discussion Paper | Discussion Paper

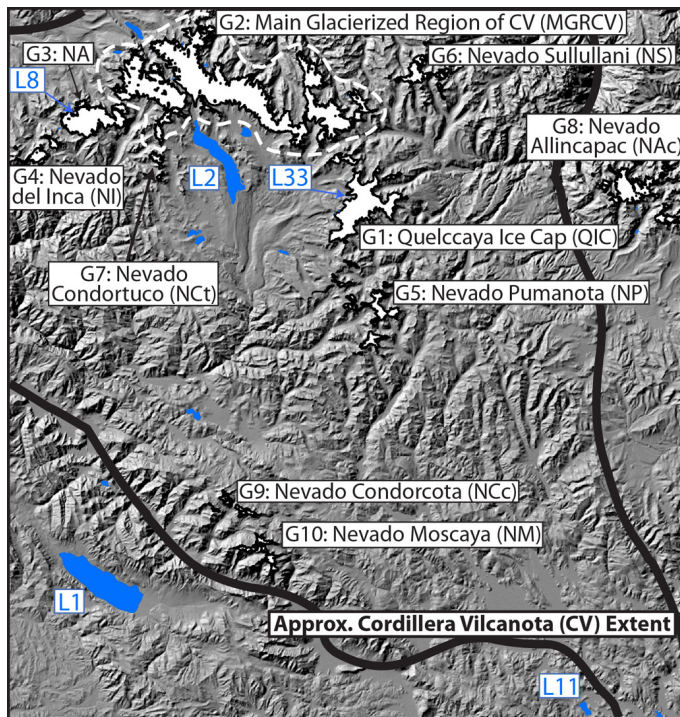


Fig. 9. Hillshade topography showing the location of the identified glacierized regions (G^*) and lakes (L^*) for which results are presented in this study. Glacierized regions are white (outlined by thin black lines), while lakes are blue (although not all 50 lakes are shown here). Some of the lakes are named: Laguna Langui (L1), Laguna Sibinacocha (L2), and Laguna Jancococota (L11). All glacierized regions have been named after the dominant peak in that region, with the exception of G2, the main glacierized region of the CV (MGRCV), the extent of which is outlined by the dashed white line. The acronym NA for G3 stands for Nevado Ausangate. Additionally, the thick black line outlines the approximate extent of the Cordillera Vilcanota. Note that Nevado Allincapac (G8) is the only glacierized region located beyond the CV.

Title Page	
Abstract	Introduction
Conclusions	References
Tables	Figures
◀	▶
◀	▶
Back	Close
Full Screen / Esc	
Printer-friendly Version	
Interactive Discussion	



Glacial areas, lake areas, and snowlines from 1975 to 2012

M. N. Hanshaw and
B. Bookhagen

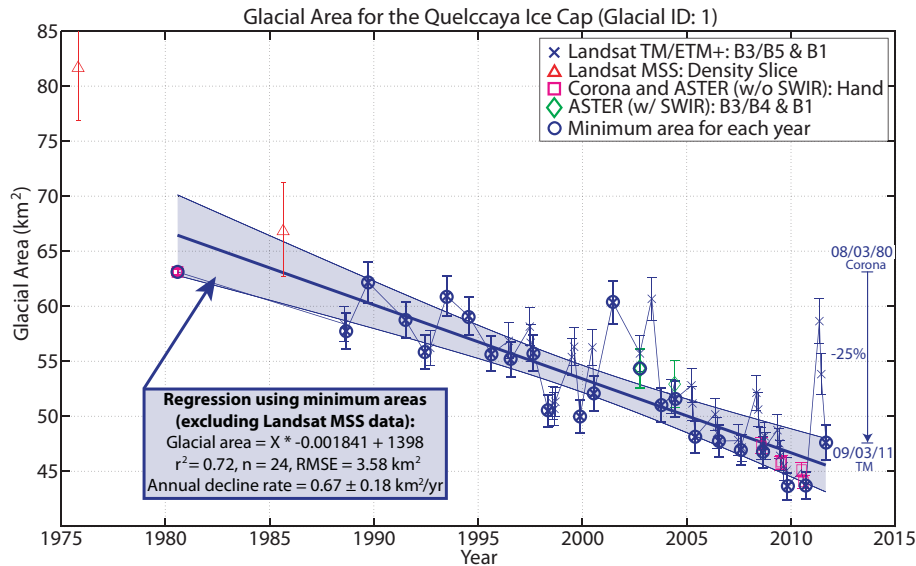


Fig. 10. Glacial-area time series for the Quelccaya Ice Cap (Glacial ID: 1, Fig. 9). Symbols indicate image type and classification method. Bold and circled data points indicate the minimum area for that year (in some cases, the only area for that year). The regression uses only these minimum areas, and shading around regression outlines 95% confidence interval (same as uncertainties for the annual decline rates).

Glacial areas, lake areas, and snowlines from 1975 to 2012

M. N. Hanshaw and
B. Bookhagen

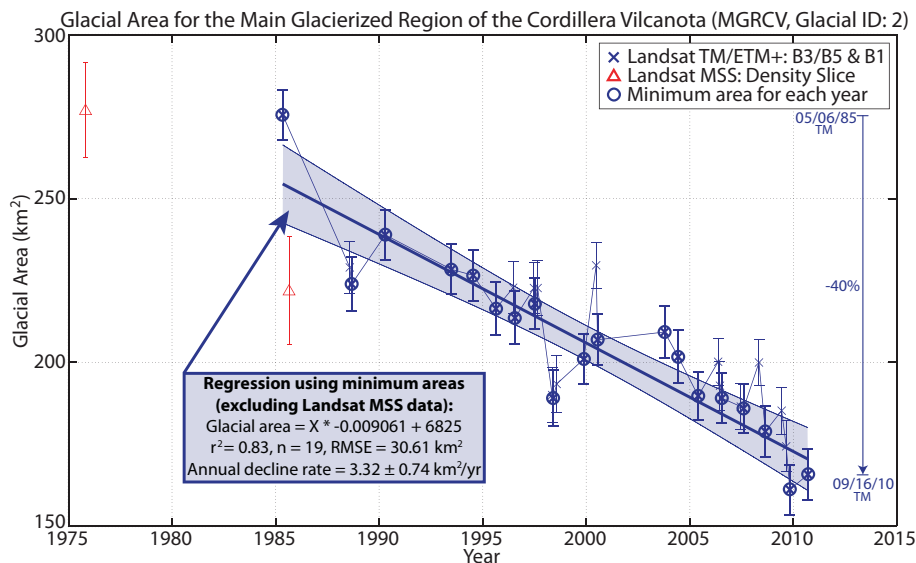


Fig. 11. Glacial-area time series for the main glacierized region of the CV (Glacial ID: 2, Fig. 9). Symbols indicate image type and classification method. Bold and circled data points indicate the minimum area for that year (in some cases, the only area for that year). The regression uses only these minimum areas, and shading around regression outlines 95 % confidence interval. As a result of the large size of this glacierized region, fewer complete satellite coverages exist because of obstruction by partial cloud cover or local snow, and therefore the number of images used for the time series and the regression is lower than for the QIC (Fig. 10).

[Title Page](#)
[Abstract](#)
[Introduction](#)
[Conclusions](#)
[References](#)
[Tables](#)
[Figures](#)
[◀](#)
[▶](#)
[◀](#)
[▶](#)
[Back](#)
[Close](#)
[Full Screen / Esc](#)
[Printer-friendly Version](#)
[Interactive Discussion](#)

Glacial areas, lake areas, and snowlines from 1975 to 2012

M. N. Hanshaw and
B. Bookhagen

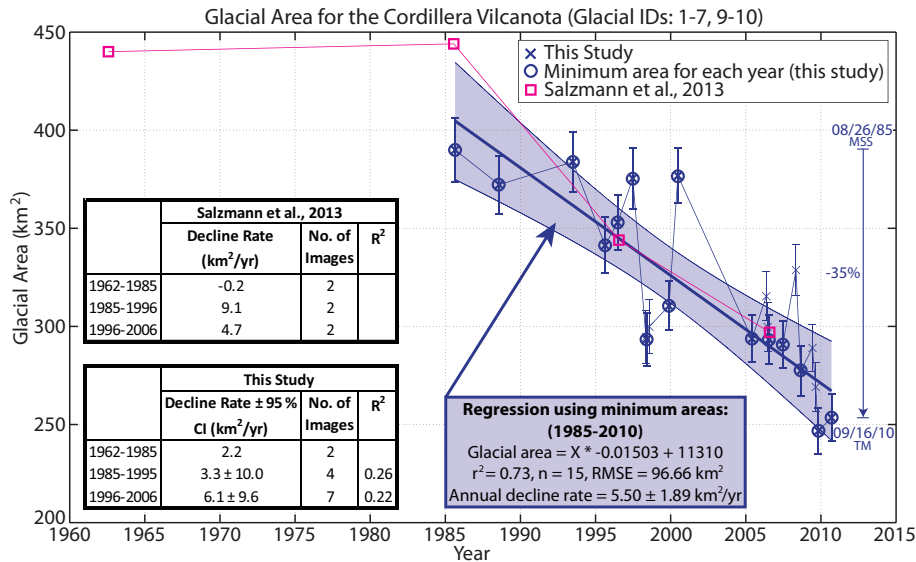


Fig. 12. Glacial-area time series for the Cordillera Vilcanota (Glacial IDs: 1–7, 9–10 combined, Fig. 9) using results from this study (blue symbols) and from Salzmann et al. (2013) (magenta squares). Their 1962 area is from Ames et al. (1989) and we have used this area also as the 1962 value in creating our 1962–1985 decline rate. Note that because these are decline rates they are listed as positive values, hence, a negative value indicates advancement. As with Figs. 10 and 11, bold and circled data points indicate the minimum area for that year (or the only area for that year). The decline rates and regression use only these minimum areas, and shading around regression outlines 95 % confidence interval.

Glacial areas, lake areas, and snowlines from 1975 to 2012

M. N. Hanshaw and
B. Bookhagen

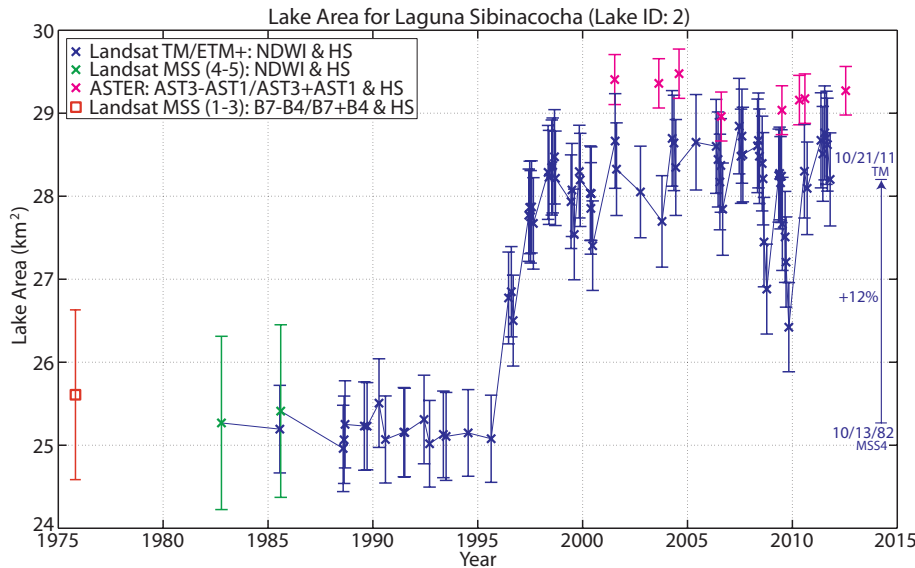


Fig. 14. Lake-area time series for Laguna Sibinacocha (Lake ID: 2, cf. Fig. 9) – a large proglacial lake.

Title Page

Abstract Introduction

Conclusions References

Tables Figures

⏪ ⏩

⏴ ⏵

Back Close

Full Screen / Esc

Printer-friendly Version

Interactive Discussion

Glacial areas, lake areas, and snowlines from 1975 to 2012

M. N. Hanshaw and
B. Bookhagen

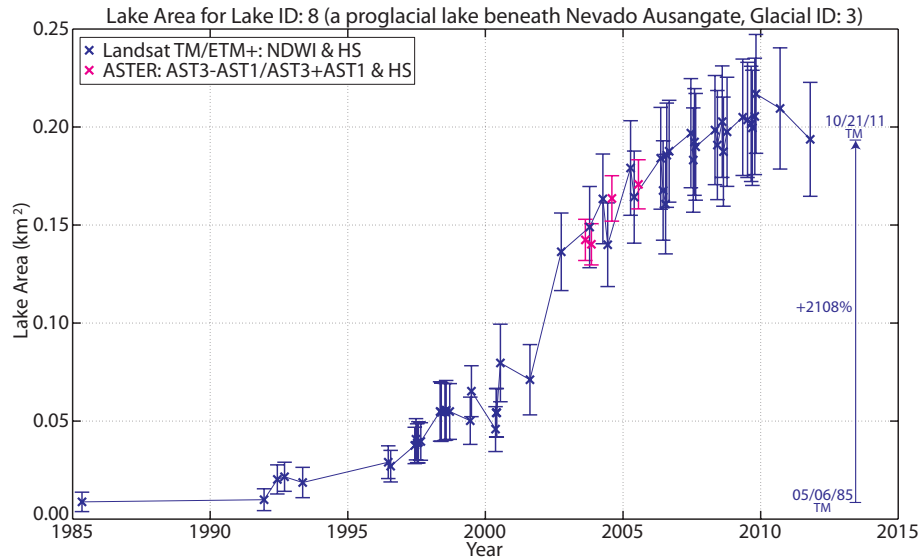


Fig. 15. Lake-area time series for Lake ID 8 (cf. Fig. 9). This proglacial lake downstream of Nevado Ausangate (Glacial ID: 3) started to rapidly grow in the late 1990s and particularly the early 2000s.

Title Page

Abstract

Introduction

Conclusions

References

Tables

Figures

◀

▶

◀

▶

Back

Close

Full Screen / Esc

Printer-friendly Version

Interactive Discussion

Glacial areas, lake areas, and snowlines from 1975 to 2012

M. N. Hanshaw and
B. Bookhagen

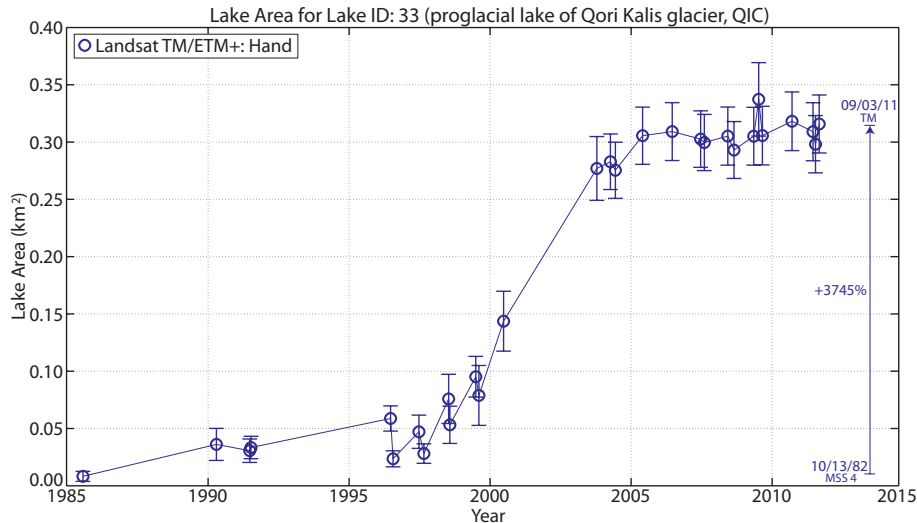


Fig. 16. Lake-area time series for Lake ID 33 (cf. Fig. 9). This proglacial lake in front of Qori Kalis glacier in the QIC (Glacial ID: 1) also started to rapidly grow in the late 1990s and early 2000s. Note that all of these measurements are hand delineated, as this lake had a spectral signature which was not captured by any of the employed methodology (cf. Fig. 5).

[Title Page](#)
[Abstract](#)
[Introduction](#)
[Conclusions](#)
[References](#)
[Tables](#)
[Figures](#)
[⏪](#)
[⏩](#)
[◀](#)
[▶](#)
[Back](#)
[Close](#)
[Full Screen / Esc](#)
[Printer-friendly Version](#)
[Interactive Discussion](#)

Glacial areas, lake areas, and snowlines from 1975 to 2012

M. N. Hanshaw and
B. Bookhagen

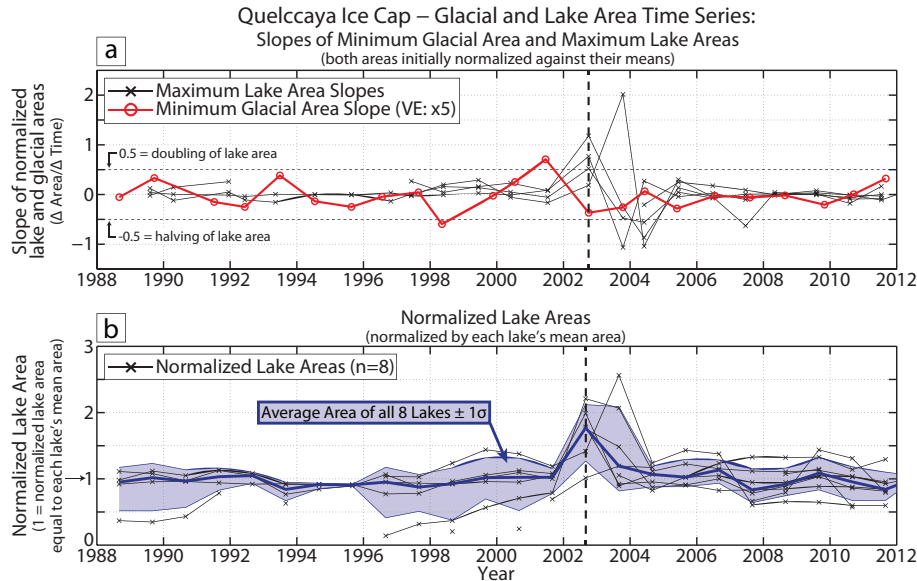


Fig. 17. Summary of glacial and lake areas for the Quelccaya Ice Cap: **(a)** slope measurements (Δ area/ Δ time between measurements of minimum glacial areas, cf. Fig. 10 (red circles, with 5x vertical exaggeration), and maximum lake areas (black crosses) for each year), with areas initially normalized against their respective means so that slopes of lakes with small areas are visible also; and **(b)** lake area time series for the 8 lakes surrounding the QIC normalized by their respective mean areas (black crosses) (i.e., a value of 1 indicates no lake area change with respect to that lake's mean area of the time series), and average lake area of all 8 lakes combined (blue line) with shading indicating $\pm 1\sigma$. Slopes **(a)** show change through time, with negative (positive) slopes indicating a decrease (increase) in area in comparison to the previous year. Note the overlap in high lake areas and slopes during 2002 (vertical black dashed lines), which correspond with a negative glacial area slope following the highest glacial area slope the previous year. We emphasize that the unusual increase in glacial area during 2001 and the subsequent rapid decline during 2002 lead to more unstable lake areas surrounding the QIC.

[Title Page](#)
[Abstract](#)
[Introduction](#)
[Conclusions](#)
[References](#)
[Tables](#)
[Figures](#)
[◀](#)
[▶](#)
[◀](#)
[▶](#)
[Back](#)
[Close](#)
[Full Screen / Esc](#)
[Printer-friendly Version](#)
[Interactive Discussion](#)

Glacial areas, lake areas, and snowlines from 1975 to 2012

M. N. Hanshaw and
B. Bookhagen

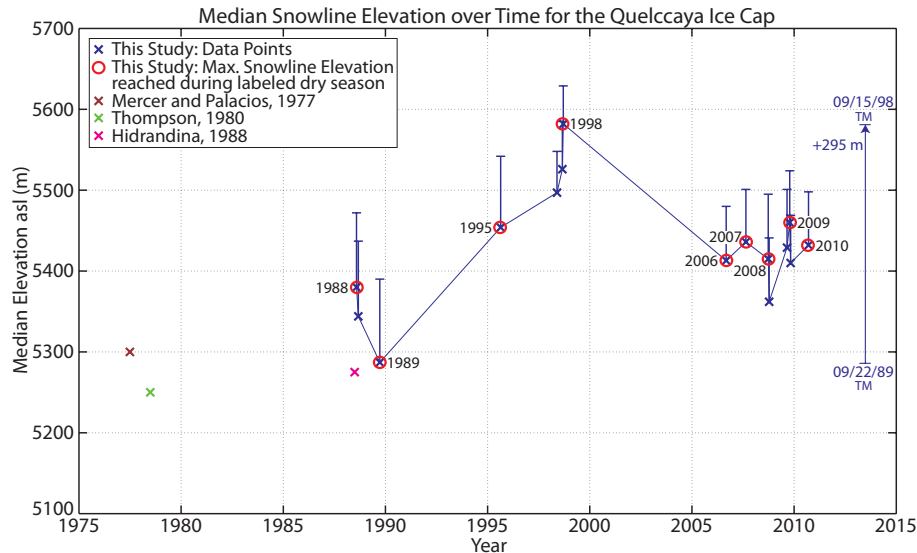


Fig. 18. Median snowline elevation against time for the QIC, including data points from other studies. Data points circled in red indicate the highest altitude that the snowline reached for that particular year (during the dry season), and represent an unvalidated estimate (likely an underestimate) of the ELA for that year. Error bars are 1σ uncertainties, and are only shown in the positive direction in response to the fact that these SLAs are minimum ELA estimates. Note that some years have multiple data points, and the maximum data points of these years are likely to be better estimates of the ELA for that year compared to those years with only one data point.

Glacial areas, lake areas, and snowlines from 1975 to 2012

M. N. Hanshaw and
B. Bookhagen

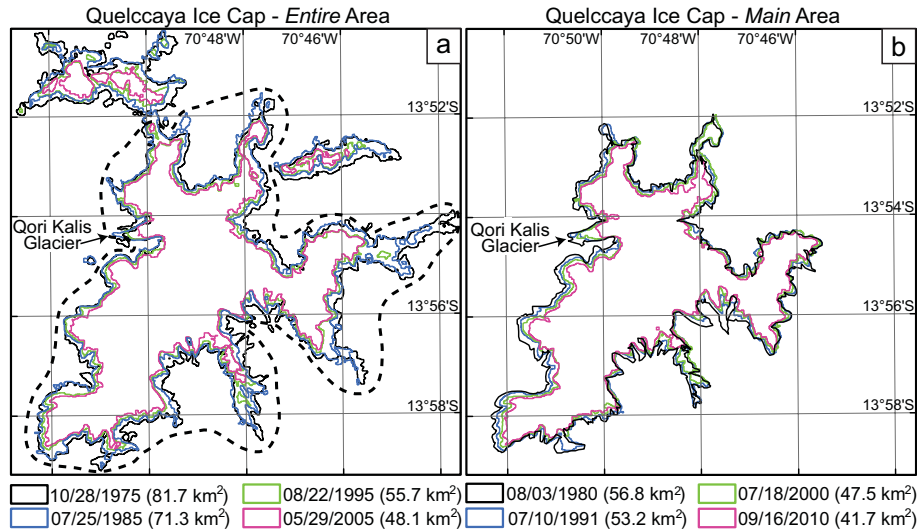


Fig. 19. Decadal outlines of the QIC from this study (see Fig. 9 for location). Decadal results (1975–2005) for the entire area of the QIC (the extent which we have used in this study) are shown in (a), while decadal results (1980–2010) for the main area only are shown in (b). Black dashed line in (a) outlines the main area shown in (b). Location of the Qori Kalis Glacier (Fig. 21) is indicated. Note that rates of retreat are not equal around the QIC.

[Title Page](#)
[Abstract](#)
[Introduction](#)
[Conclusions](#)
[References](#)
[Tables](#)
[Figures](#)
[◀](#)
[▶](#)
[◀](#)
[▶](#)
[Back](#)
[Close](#)
[Full Screen / Esc](#)
[Printer-friendly Version](#)
[Interactive Discussion](#)

Glacial areas, lake areas, and snowlines from 1975 to 2012

M. N. Hanshaw and
B. Bookhagen

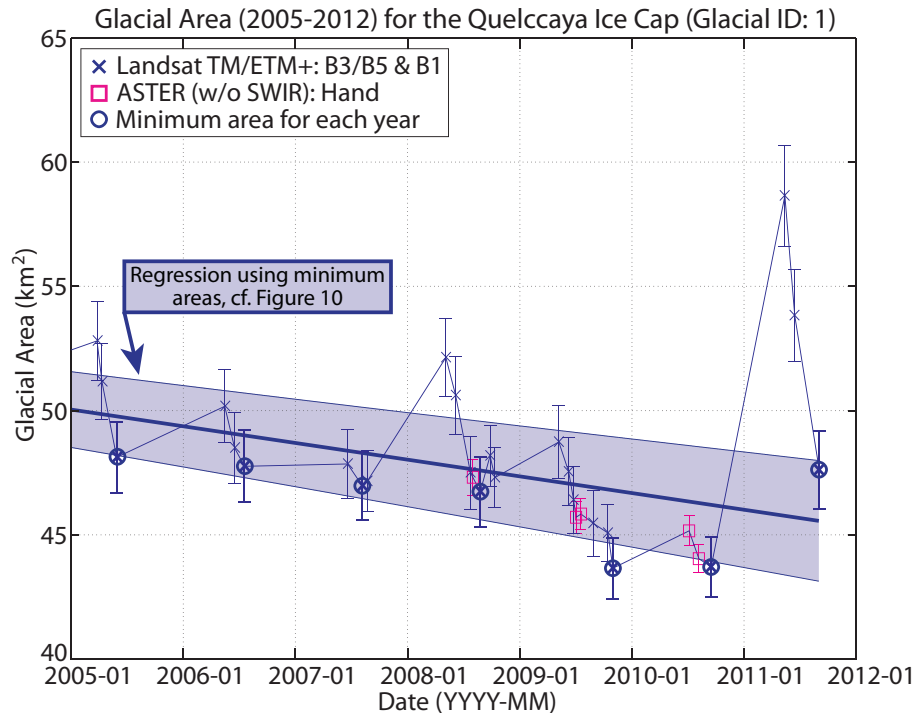


Fig. 20. Focus on 2005–2012 of the glacial-area time series for the Quelccaya Ice Cap (the whole time series is shown in Fig. 10). Symbols indicate image type and classification method. We emphasize the large variation of glacial area during one year, specifically over the course of the dry season (roughly April/May through September/October) as images are dominantly from this period.

Glacial areas, lake areas, and snowlines from 1975 to 2012

M. N. Hanshaw and
B. Bookhagen

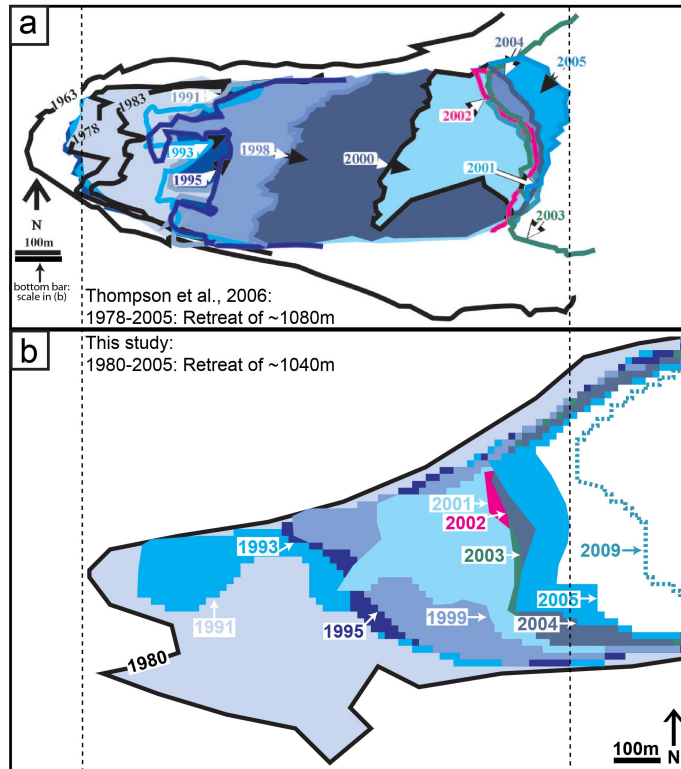


Fig. 21. Retreat of the Qori Kalis glacier in the QIC from **(a)** 1963 to 2005 (figure modified after Thompson et al., 2006) and **(b)** 1980 to 2009 (results from this study). This comparison shows field-based measurements **(a)** and our satellite-based measurements **(b)**. Dashed lines are used for ease of viewing beginning and ending glacier extents in 1978 and 2005.

Title Page	
Abstract	Introduction
Conclusions	References
Tables	Figures
◀	▶
◀	▶
Back	Close
Full Screen / Esc	
Printer-friendly Version	
Interactive Discussion	

Glacial areas, lake areas, and snowlines from 1975 to 2012

M. N. Hanshaw and
B. Bookhagen

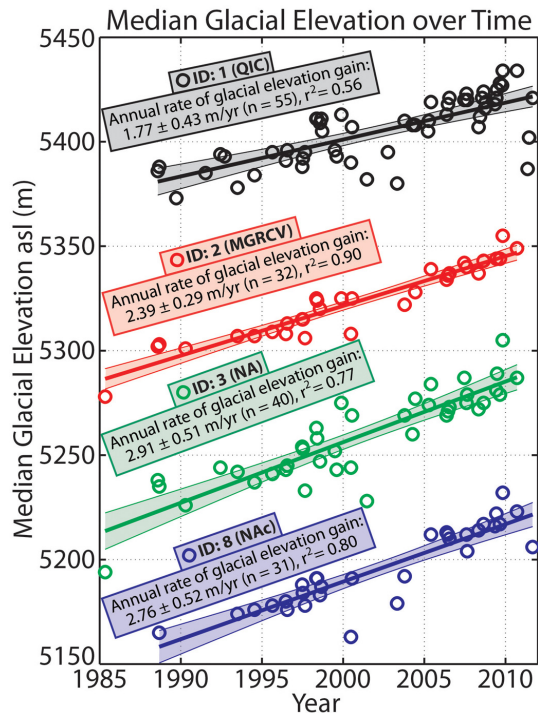


Fig. 22. Median glacial elevation ($\pm 95\%$ confidence interval) against the time series of this study for the 4 largest glacierized IDs in this region (IDs 1: Quelccaya Ice Cap (QIC), 2: Main Glacierized Region of the CV (MGRCV), 3: Nevado Ausangate region (NA), and 8: Nevado Allincapac region (NAC), a glacierized area just beyond the eastern boundary of the CV).

Title Page

Abstract

Introduction

Conclusions

References

Tables

Figures

◀

▶

◀

▶

Back

Close

Full Screen / Esc

Printer-friendly Version

Interactive Discussion

Glacial areas, lake areas, and snowlines from 1975 to 2012

M. N. Hanshaw and
B. Bookhagen

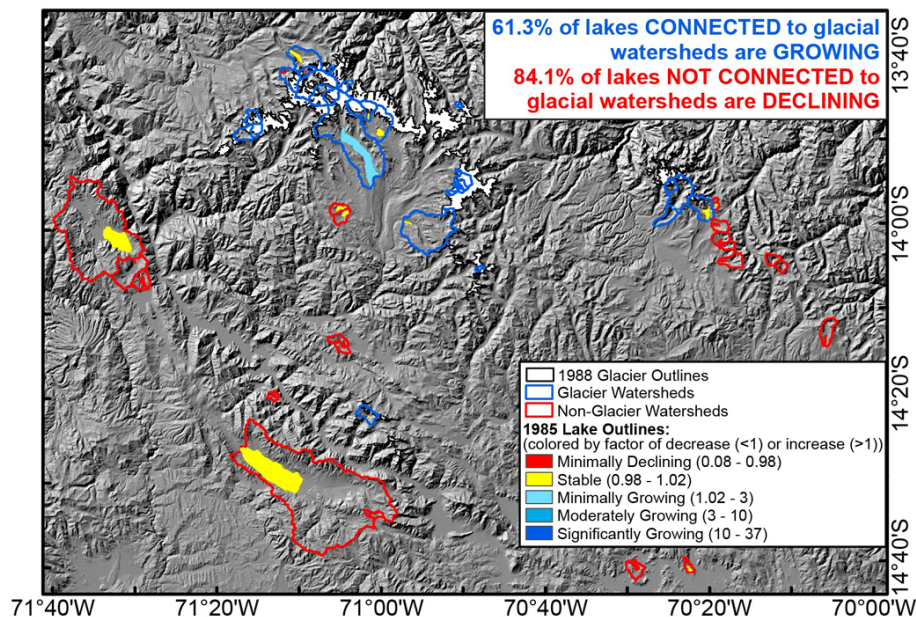


Fig. 23. Regional trends in lakes throughout the study area, indicating whether the lake (based on most recent area) is stable (0.98–1.02), declining (< 1) or growing (> 1) in relation to its earliest Landsat TM area. Glacial watersheds are delineated in blue, and non-glacial watersheds are delineated in red. The SRTM DEM hillshade is shown in the background, and glacial regions are in white and outlined in black.

Title Page

Abstract

Introduction

Conclusions

References

Tables

Figures

⏪

⏩

◀

▶

Back

Close

Full Screen / Esc

Printer-friendly Version

Interactive Discussion

Glacial areas, lake areas, and snowlines from 1975 to 2012

M. N. Hanshaw and
B. Bookhagen

Title Page

Abstract

Introduction

Conclusions

References

Tables

Figures

◀

▶

◀

▶

Back

Close

Full Screen / Esc

Printer-friendly Version

Interactive Discussion

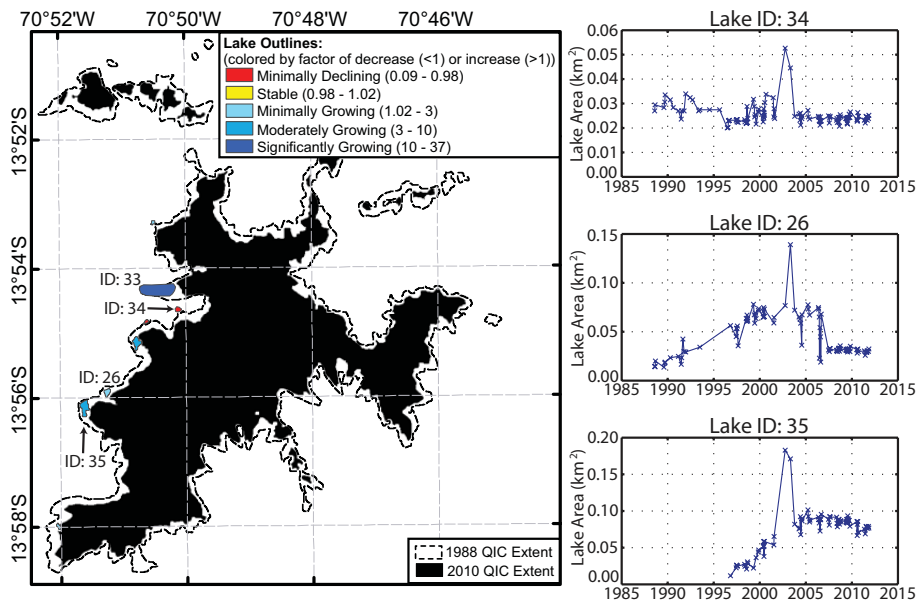


Fig. 24. Regional trends in lakes surrounding the QIC, indicating whether the lake (based on most recent area) is stable (0.98–1.02), declining (< 1) or growing (> 1) in relation to its earliest Landsat TM area. Here, we also indicate the extent of the QIC in 1988 (dashed black outline) and 2010 (solid black). Lake IDs indicate those lakes for which specific lake area results are shown in this figure or manuscript text, however, all 8 of these lakes are those for which results are reported in Fig. 17. Time series results shown here use only Landsat TM/ETM+ (NDWI & HS) data points. We associate the rapid lake-area increase during 2002–2003 with enhanced melting during that season and the season prior.